REPORT NO. 60

MAY, 1952

THE COLLEGE OF AERONAUTICS

CRANFIELD

An investigation of the Flexure-Torsion Flutter characteristics of aerofoils in cascade

-by-

G.M. Lilley, M.Sc., D.I.C., A.F.R.Ae.S.

of the Department of Aerodynamics

SUMMARY

Part 1 of this report describes the results obtained from a series of tests on the flexure-torsion flutter characteristics of cascades of similar aerofoils having symmetrical sections. The critical flutter speeds and frequencies of the aerofoils in cascade have been compared with their isolated values. The investigation has included the effects of gap-chord ratio and of stagger. The Reynolds number, based on wing chord, was about 0.15×10^6.

It was found that the critical flutter speed decreased as the gap-chord ratio was reduced. The variation of critical flutter speed with stagger angle was relatively small. In both cases the critical flutter frequency was greater than that for the isolated aerofoils. It was noted that during flutter adjacent aerofoils were oscillating approximately 180° out of phase, and hence alternate blades were in phase. The mode of oscillation was of the flexure-torsion type.

The accuracy of the experiments was limited by slight variations in the structure of the models and in the case of the wooden aerofoils, by noticeable changes in their torsional and flexural stiffnesses with humidity and temperature.

/Part 2 ...

MEP

Part 2 of this report is a review of the theoretical studies on oscillating aerofoils in cascade. Since, as is noted in Part 1, adjacent aerofoils vibrated 180° out of phase, the problem is analoguous to that of a single oscillating aerofoil placed between parallel walls. The air forces have been calculated approximately enabling the flutter characteristics of the aerofoils, described in Part 1, to be computed and a comparison made with the experimental results. Fair agreement has been obtained, and such differences as there are, it is suggested, are due to the neglect of the effects of finite aspect ratio and thickness of the aerofoils and the rigid body movements. The latter problem together with an account of simplified flutter calculations are discussed in appendices.

The major part of the experimental work discussed in Part 1 was reported by K. Alming, G.E. Gadd and W.F. Wiles in an unpublished note.

I N D E X

			Page
		Notation	5
Part 1	§1	Introduction	9
	§2	Apparatus	10
	§3	Test Procedure	11
	§4	Experimental results	12
	§5	Discussion	16
	§6	Acknowledgements	18
	§7	Conclusions	18
Part 2	§1	Introduction	20
	§2	General theory	22
	§3	Flutter with a single degree of freedom	36
		References	38

Appendices

1. The calculation of the critical flutter speed and frequency 40
2. Finite amplitude effects 46

Figures

1. View of the tunnel showing the unstaggered cascade in position
2. Back of the turntable showing blocks for clamping the aerofoils
3. Cascade of aerofoils with stops in position
4. General view of the metal blade
5. View of the aerofoil mounted on the vibration table
6. Decline in flutter speed with age
7. Critical flutter variation with gap-chord ratio
8. Flutter speed variation with stagger angle

/9. ...

9. Variation of critical flutter frequency with gap-chord ratio

10. Variation of critical frequency with gap-chord ratio and stagger angle

11. Variation of the critical flutter speed with gap-chord ratio for the unstaggered cascade

12. Variation of the reduced frequency with gap-chord ratio for the unstaggered cascade

13a Aerofoils in cascade $\frac{s}{c} = 0.5 \quad \sigma = 15^{\circ}$

13b " " " " $\sigma = 0^{\circ}$

13c Isolated aerofoil $\alpha = 0^{\circ}$

14a Mode in flexure

14b Mode in torsion

15a
Notation
15b

16. Variation of A and B with gap-chord ratio

17. Variation of the parameter q with gap-chord ratio

18. Variation of the functions Q_1, Q_2, Q_3, Q_4

19. Typical values of the classical aerodynamic derivatives

20. Notation for flutter calculations

21. Typical variation of the coefficient c_1 with α and k_1

22. Diagram showing aerofoils in cascade.

NOTATION

A		real part of C (see below)
A_1		flexural moment of inertia
a_1		non-dimensional form of A_1
A_3		flexural-torsional product of inertia
a_3		non-dimensional form of A_3
b	$\equiv$	$\tilde{\omega}s/2\pi c$
B		imaginary part of C (see below)
B_1		direct flexural damping coefficient
b_1		non-dimensional form of B_1
B_3		compound torsional damping coefficient
b_3		non-dimensional form of B_3
C_1		flexural stiffness
c_1		non-dimensional form of C_1
c		chord
C ($\equiv A-iB$)		generalised Theodorsen function
C_3		torsional cross-stiffness
c_3		non-dimensional form of C_3
$E(k)$		complete elliptic integral of the second kind
f		frequency
$f(\eta)$		flexural mode
$F(\eta)$		torsional mode
$F(a,b;c,z)$		hypergeometric function
G_1		flexural-torsional product of inertia
g_1		non-dimensional form of G_1
G_3		torsional moment of inertia
g_3		non-dimensional form of G_3
hc		distance of flexural axis from leading edge
$H_1^{(2)}, H_o^{(2)}$		Hankel functions
J_1		compound flexural damping coefficient
j_1		non-dimensional form of J_1

/J_3 ...

J_3		direct torsional damping coefficient
j_3		non-dimensional form of J_3
k	$\equiv$	$\tanh \lambda$
k'	$\equiv$	$\sqrt{1 - k^2}$
$K(k), K'(k)$		complete elliptic integrals of the first kind
K_1		flexural cross-stiffness
k_1		non-dimensional form of K_1
K_3		direct torsional stiffness
k_3		non-dimensional form of K_3
L		flexural moment
ℓ		span
ℓ_ϕ		flexural stiffness
$\ell_z\ \ell_{\dot{z}}\ \ell_{\ddot{z}}$		aerodynamic derivatives
$\ell_\theta\ \ell_{\dot{\theta}}\ \ell_{\ddot{\theta}}$		aerodynamic derivatives
M		pitching moment; torsional moment; Mach No. in free stream
m		mass/unit length of span
m_θ		torsional stiffness
$m_z\ m_{\dot{z}}\ m_{\ddot{z}}$		aerodynamic derivatives
$m_\theta\ m_{\dot{\theta}}\ m_{\ddot{\theta}}$		aerodynamic derivatives
p		pressure
$Q_1 Q_2 Q_3 Q_4$		functions of q
q	$\equiv$	$\exp(-\pi K'/K)$
$q_o q_1 q_2 q_3 q_4$		dimensional coefficients
$\bar{q}_o \bar{q}_1 \bar{q}_2 \bar{q}_3 \bar{q}_4$		non-dimensional coefficients
r_n		distance (see eqn. 2.22)
$r_1 r_2 r_3 r_4$		coefficients in flutter equations
$R_1 R_2 R_3$		coefficients in flutter equations
s		gap
t		aerofoil thickness; time
u		perturbation velocity component in direction OX
V		freestream velocity - isolated aerofoil
V'		freestream velocity - aerofoil in cascade
w		perturbation velocity component in direction OZ

/x ...

x		coordinate in chordwise direction
x_f		distance of reference section from origin
y		coordinate in spanwise direction
Z		force in direction OZ
z		coordinate normal to chord
$\mathfrak{z}$		aerofoil displacement in direction OZ
$\alpha \equiv \frac{1}{k} \tanh \lambda x$,		angle of incidence; aerodynamic stiffness parameter
β	$\equiv$	$\exp(\pi c/s)$; elastic stiffness parameter
γ		bound vorticity; phase angle
γ_n		coefficient in series $Q_3 Q_4$
Γ		circulation
ε		free vorticity
η	$=$	y/ℓ
θ		aerofoil rotation; torsional coordinate
ϑ	$\equiv$	$\theta c/\ell$
K_c		radius of gyration
λ	$\equiv$	$\frac{\pi c}{2s}$
$\lambda_\phi \lambda_{\dot\phi} \lambda_{\ddot\phi}$		aerodynamic derivatives
$\lambda_\theta \lambda_{\dot\theta} \lambda_{\ddot\theta}$		aerodynamic derivatives
$\mu_\phi \mu_{\dot\phi} \mu_{\ddot\phi}$		aerodynamic derivatives
$\mu_\theta \mu_{\dot\theta} \mu_{\ddot\theta}$		aerodynamic derivatives
ν		kinematic viscosity
ξ	$\equiv$	x/c
$c\bar{\xi}$		distance of the centre of gravity from the leading edge
$c\tilde{\xi}$		distance of the flexural axis from the leading edge
$\tilde{\omega}$	$\equiv$	$\omega c/V$ frequency parameter (reduced frequency)
ρ		air density
σ		stagger angle
τ	$\equiv$	$\gamma + \varepsilon$
ϕ		flexural coordinate; velocity potential
Φ		acceleration potential
ω		circular frequency
ω_f		natural frequency in flexure

/ω_t ...

ω_t natural frequency in torsion

Suffix c denotes the value of a quantity at which flutter is just maintained.

Suffix o denotes the free stream value.

§1. Introduction

The effect of the interference of adjacent blades in a cascade of aerofoils in modifying the isolated critical flutter characteristics of the aerofoils has received little attention. A recent paper by Bellenot and Lalive d'Epinay (reference 1) describes some tests on cascade flutter made at one gap-chord ratio over a range of stagger angles. They found that the modes of vibration during flutter were either pure torsion or pure flexure and these are therefore different from the type of flutter investigated in this report. In Part 2 of the present paper the problem of flutter with one degree of freedom is discussed.

An experimental investigation of the flutter characteristics of aerofoils in cascade has been conducted in the Aerodynamics Laboratory of the College of Aeronautics between 1948 and 1950. Two types of model aerofoils have been used in these experiments

(a) Aerofoils manufactured from a light wooden framework covered with doped silk

(b) Rigid metal aerofoils supported from combined flexure and torsion springs at the root.

The two types of aerofoils had approximately the same chord but the spans were different. It was found, however, that there was in the main qualitative agreement between the two sets of results. Therefore, in order to avoid confusion and undue repetition, and noting that the aerofoils of type (a) are more allied to practical aerofoils, only the results obtained from type (a) aerofoils will be presented here. The small differences in the flutter characteristics obtained between aerofoils of types (a) and (b) have not been completely explained but it is considered that these differences are probably due to the variations in the end fixing, the modes of vibration and the aspect ratio.

The accuracy of these experiments was limited for reasons which will be discussed.

The major part of the experimental work, relating to the wooden aerofoils, described in this report was reported by K. Alming, G.E. Gadd and W.F. Wiles in an unpublished note. The experiments on the metal aerofoils were completed by E.S. Farris, E.T.B. Smith and C.G. Hughes.

§2 ...

§2. Apparatus

The experiments were conducted in a blower type wind tunnel, whose working section dimensions were 18.75in. x 8.75in. and the speed range was zero to 170 feet per second. The distribution of velocity across the working section outside the boundary layer was uniform to within ± 0.5 per cent.

The aerofoils were cantilevered from a turntable in a side wall extension to the wind tunnel contraction (see figures 1 and 2). The wooden aerofoils were of rectangular planform, 3in. chord and 8in. span, and were of NACA 0010 section. Each aerofoil had a mahogany spar 0.15in. square and eight mahogany ribs each 0.10in. thick. The framework was covered with silk which was doped with a mixture of vaseline and chloroform. The blades were provided with stops (see figure 3) in order to limit the amplitude of the blades during vibration.+

The metal aerofoils were first made of solid light alloy. They had a 14 per cent thick symmetrical section, a chord of 2.9in. and a span of 2.9in. The blades were fixed to various forms of spring hinges connected to the working section turntable. The flexure-torsion springs were designed so that the natural frequencies of the blades in flexure and torsion were nearly the same as those of the wooden aerofoils. Although many different types of springs were tested they all quickly failed by fatigue. A second set of metal aerofoils were manufactured from 30 s.w.g. brass sheet, the aerofoil section being the same as for the solid blades but the span was increased to 6in. Separate flexure and torsion springs were fitted and friction was reduced to a negligible amount by the use of taper needle roller bearings. (See figure 4).

The wind speed in the working section was calibrated against static pressure tappings in the contraction section and the settling chamber. The frequency of the oscillating aerofoils was measured using a strobo-tachometer having an error of

/less than ...

+ The stops were provided to prevent damage to the blades when they were fluttering above their critical speeds. In all cases when the blades were fluttering at or near to their critical speeds, and the amplitudes of the oscillations were therefore small, the stops could be removed.

less than 1 cycle per second.

The torsional and flexural stiffnesses of the aerofoils were measured by applying torques and loads respectively about and at the flexural axis at the tip section. The natural frequencies in torsion and flexure were measured on a standard vibrating table (see figure 5).

A film showing the motion of the aerofoils during flutter was taken with a cine camera, f1.5, 8 frames per second, using stroboscopic light.

§3. Test Procedure

Each aerofoil was tested separately and its critical flutter speed and frequency were noted. These were obtained by increasing the wind speed until flutter commenced; the wind speed was then decreased until flutter stopped. The wind speed just prior to the blade flutter stopping was recorded as the critical value. The frequency could not, however, be conveniently obtained corresponding to the critical wind speed. Consistent readings of the critical frequency were, however, obtained by measuring the frequency at each steady wind speed above the critical wind speed. Since the latter was obtained as stated above the critical frequency could easily be obtained by extrapolation (see figure 9).

The aerofoils were then selected so that a cascade of blades could be found such that the isolated characteristics of the aerofoils differed by less than $\pm$ 5 per cent. The aerofoils were arranged in cascade so that the weakest aerofoils were near the centre. The critical flutter speed and frequency were taken corresponding to the mean values of these quantities obtained from the three central aerofoils. In the case of the wooden aerofoils the critical flutter speed decreased with blade age owing to fatigue. The flutter characteristics were also dependent on the prevailing temperature and humidity. It was therefore necessary to measure the isolated aerofoil characteristics immediately before and after a test (at a given gap-chord ratio).

In order to reduce the magnitude of the air forces and amplitudes of the aerofoils during flutter, the aerofoils

/were in ...

were in all cases set at zero incidence relative to the upstream direction. A few measurements were, however, made at 5° incidence and since no change in the flutter characteristics could be detected it was assumed that the blade incidence was not a very important parameter at least in the range $\pm 5^{\circ}$.

It was noted that when fluttering, adjacent aerofoils were approximately 180° out of phase, and hence with zero stagger, they might be regarded as images of each other in a rigid plane boundary midway between them.

The above measurements were, therefore, repeated for the case of a single aerofoil placed midway between two parallel plates. The gap between the plates was varied; the distance apart of the plates being assumed to correspond to the gap between adjacent aerofoils when in cascade, but with zero stagger.

§4. Experimental results

The fall of the critical flutter speed with age is shown in figure 6. The temperature and humidity variations have also been plotted on figure 6 and it is seen that little correlation was obtained with the changes in the flutter speed. This does not necessarily indicate that temperature and humidity do not affect the flutter characteristics but rather that fatigue of the flexible wooden structure was probably predominant. Further tests did in fact show that the elastic stiffnesses, especially the torsional stiffness, were altered by changes in temperature and humidity. It was also found that the porosity of the silk covering was not always uniform and extreme care was required in applying the chloroform-vaseline dope. It was therefore concluded that changes in the critical flutter speed were mainly caused by the wooden structure and the silk covering 'drying out' (at the beginning of each test). The overall effects of blade fatigue, and room temperature and humidity, were reduced to a minimum by the experimental procedure discussed in the previous paragraph.

The variation of the critical flutter speed of the cascade of aerofoils with the gap-chord ratio is shown in figure 7. The results of tests on a single aerofoil placed between parallel plates is also included. The blockage curve shows the ratio of the measured wind speed upstream of the cascade

/compared ...

compared with the mean speed in the gaps between adjacent aerofoils. It is clearly seen that the very large decrease in the critical flutter speed with gap-chord ratio cannot be entirely due to a blockage effect.

The results of the two tests can be expressed by the following empirical law

$$\frac{V'_c}{V_c} = 1 - \frac{1}{(1+s/c)^n}$$

where

n = 4.24 for the aerofoil in cascade
= 3.15 for the single aerofoil between two parallel plates

V'_c = the critical flutter speed of an aerofoil in cascade

V_c = the critical flutter speed of the isolated aerofoil

s/c = gap-chord ratio.

The effect of the cascade stagger angle on the critical flutter speed of the aerofoils is shown in figure 8. It is seen that the critical flutter speed is nearly independent of stagger angle.

The frequency-speed curves for different gap-chord ratios of the aerofoils are shown in figures 9a and 9b; the former shows the results obtained from a single aerofoil placed between two parallel plates whilst the latter shows the results for an unstaggered cascade of five aerofoils. The dotted lines show the variation of frequency with wind speed when the aerofoils are fluttering above their critical wind speeds. The blacked in points correspond to the extrapolated critical frequencies (see paragraph 3 above) at each gap-chord ratio. It is seen that again the results are similar in the two cases and that the critical frequency of the aerofoil in cascade is only slightly greater than that of the single aerofoil between plates. The corresponding effects with cascade stagger angle are shown in figure 10. The critical flutter frequency increases with stagger angle although the increase is not large for stagger angles below 20°. It was observed that for small gap-chord ratios the frequency increased rapidly for small increases above the critical flutter speed. This fact probably accounts for the scatter of the observed points for s/c equal to 0.25 in figure 10.

/The ...

The experimental results for the unstaggered cascade are compared with the theoretical values, obtained from Part 2, in figures 11 and 12. In figure 11 the square of the critical speed ratio has been plotted against gap-chord ratio. Good agreement between theory and experiment is obtained except at the smallest value of gap-chord ratio. This is not surprising since the finite amplitude and the effect of the aerofoil thickness, which have both been neglected in the theory, will increase in importance as the gap-chord ratio decreases. In figure 12 the square of the reduced frequency ratio has been plotted against s/c. Good agreement between the observed and theoretical values is again obtained except at the lowest value of gap-chord ratio. This agreement between theory and experiment is encouraging but not conclusive, since the theoretical values do not agree so well with the results obtained from the tests on the single aerofoil between parallel plates. Nevertheless, the theory should apply equally well to both systems, provided that the aerofoils in cascade are vibrating exactly in antiphase, and hence further investigation of these differences is desirable.+

Figure 13 shows a series of photographs taken in stroboscopic light for a cascade having a gap-chord ratio of 0.5 and two stagger angles $\sigma = 0^{\circ}$ and 15°. The corresponding pictures taken for an isolated aerofoil are also given. The antiphase motion between adjacent aerofoils is clearly indicated. The motion, in detail, can be described as follows.-

(i) An aerofoil in its mid-position and moving upwards say, has a positive twist i.e. its leading edge is above its trailing edge.

(ii) As the motion progresses the twist is reduced until

/at the ...

+ These differences may be accounted for as follows.-

(i) The aerofoils in a cascade had isolated flutter characteristics which differed by about $\pm$ 5 per cent, and experimental inaccuracies of at least $\pm$ 5 per cent will therefore exist.

(ii) In the case of the single aerofoil oscillating between parallel plates the boundary layers adjacent these plates may produce important changes in the flow even though a rough calculation has shown that the equivalent blockage effect is small.

at the point of maximum flexure the twist is approximately zero or slightly negative.

(iii) As the aerofoil starts its downward path its twist becomes more negative reaching a maximum at about the mid-position of the flexural displacement.

(iv) As the flexural motion proceeds downwards the twist of the aerofoil is reduced and reaches zero or a slightly positive value at the position of maximum negative displacement.

(v) Whilst the motion described in (i) is taking place the aerofoil above is moving downwards with negative twist which is decreasing as the flexural motion progresses.

(vi) Similarly the aerofoil below is also moving downwards with negative twist which is decreasing as the flexural motion progresses.

Hence alternate aerofoils in a cascade, both unstaggered, have similar motions. Their motion corresponds to the classical flexure-torsion vibrations in which the torsional motion lags behind the flexural motion (see reference 2).

The type of motion discussed above was present for all arrangements of aerofoils except that at angles of stagger above 35° the flutter amplitude did not remain constant. In this case a pulsation of the aerofoil was superimposed on the steady oscillations. The reasons for this require further investigation.+

The measured elastic stiffnesses and the natural frequencies of uncoupled flexural and torsional vibrations in still air varied for each aerofoil in the cascade. Typical values for the central aerofoil in the cascade together with its isolated flutter characteristics are given below in Table 1.

/Table 1 ...

+ 'Pulsating flutter' of the type encountered at large angles of stagger is probably due to the disturbances created by the oscillatory wakes affecting the motions of adjacent aerofoils. In the case of small angles of stagger the fluttering aerofoils are moving towards the surfaces of adjacent aerofoils, but at large angles of stagger the fluttering aerofoils are moving during one half of their motion towards relatively undisturbed air, whilst on the other half they are moving towards the disturbed wakes of adjacent aerofoils.

TABLE 1

Quantity	Symbol	Measured Value
Flexural stiffness	l_ϕ	2.49 lb.ft./radian
Natural flexural circular frequency	ω_f	152 rad./sec.
Distance of flexural axis from the leading edge	hc	0.25 c
Torsional stiffness	m_θ	0.15 lb.ft./radian
Natural torsional circular frequency	ω_t	326 rad./sec.
Critical flutter speed (isolated aerofoil)	V_c	87.0 f.p.s.
Critical flutter circular frequency	ω_c	220 rad./sec.
Reduced frequency	$\tilde{\omega} \equiv \frac{\omega_c c}{V_c}$	1.0
Reynolds number	$\frac{V_c c}{\nu}$	1.37×10^5

From the results quoted in Table 1 above and the results plotted in figure 9 it can be seen that the critical flutter frequency increases towards the natural frequency in torsion as the gap-chord ratio is reduced.

The modes in flexure and torsion, obtained from static tests, are shown in figures 14a and 14b respectively.

§5. Discussion

The main reason for the decrease in critical flutter speed with gap-chord ratio arises from the increased negative value of the aerodynamic torsional-stiffness derivative, (see Part 2) even though the corresponding variations of the aerodynamic torsional and flexural damping derivatives are many times greater. It was first thought that the reduction in the critical flutter speed was due to the aerodynamic forces and moments which arise when the displacements of adjacent aerofoils in the cascade are not infinitesimal. It is shown in Appendix 2 that these forces and moments arising from rigid body movements are inversely proportional to the gap-chord ratio. The

/numerical ...

numerical value of the results given in Appendix 2 are unlikely to be correct owing to the drastic nature of the assumptions used. However, even with these values of the aerodynamic derivatives added algebraically to those calculated from the 'classical theory' of Part 2, the critical flutter speeds and frequencies were changed but slightly from the values calculated using only the derivatives of the 'classical theory'.

The aerodynamic forces which arise due to the rigid body movements (even though these may be relatively small compared with, say, the gaps between adjacent aerofoils) are important however in controlling the type of antiphase flutter occurring between adjacent blades in a cascade. The aerodynamic forces and ensuing motions probably arise as follows. When a given aerofoil in a cascade is vibrating with a harmonic motion of small amplitude in an otherwise steady airstream, the air velocity over its upper and lower surfaces will respectively increase and decrease as it pursues say the upward part of its motion, since if we assume that initially the adjacent aerofoils, above and below it, are at rest the effective upper and lower gaps will respectively decrease and increase due to the aerofoil motion. But the increase in velocity over the top surface of the given aerofoil will also exist over the lower surface of the adjacent upper aerofoil on which in consequence a normal force in the downward direction will be induced. Similarly a downwards induced force will be exerted on the adjacent lower aerofoil. These induced forces will be sinusoidal and vibration of these aerofoils will therefore be excited by the oscillations of the parent aerofoil and the motions of these aerofoils will be in the opposite phase to that of the parent aerofoil. It appears therefore that the structurally weakest aerofoil in a cascade of aerofoils will commence fluttering at a critical speed determined by its elastic stiffnesses, inertias and the aerodynamic derivatives calculated from the 'classical theory' (see Part 2). This aerofoil will in turn excite the adjacent aerofoils.

The corollary to be gained from this explanation is that the critical flutter speed of a cascade of aerofoils is that corresponding to the structurally weakest member in the cascade provided that the variations in the elastic stiffness are not very large.

The variation of the critical flutter speed with gap-chord ratio, as determined in this paper, is not a universal

/curve ...

curve for all cases of aerofoil geometry, elastic stiffness, and inertia. The results, as quoted, apply only to the particular type of aerofoil tested and each particular arrangement requires a separate investigation.

The good agreement between theory and experiment for gap-chord ratios greater than 0.5 suggests that future work on the compressible flow problem at high subsonic Mach numbers, following on similar lines to that suggested in Part 2 of this paper, is worthy of consideration.

§6. Acknowledgements

This work was initiated by Professor W.J. Duncan who directed it in the important early stages. During the course of the investigation stimulating discussions were held with Professor A.D. Young and other members of the staff of the Department of Aerodynamics.

Thanks are due to Dr. S. Kirkby who checked certain sections of Part 2 of this paper and to Mr. S.W. Ingham who was responsible for some of the numerical calculations.

The wooden aerofoils were manufactured by Mr.C.D.Bruce and Mr. S.H.Lilley constructed the metal aerofoils and spring arrangements. Some of the later experimental data on the wooden aerofoils were obtained by Messrs. A.R.McLean and J.Bowles.

§7. Conclusions

1. Experimental results have shown that when aerofoils are placed in cascade, at small incidence, their critical flutter speeds are reduced compared with their isolated values. Similarly the frequency of the flexure-torsion vibrations, at the critical flutter speed, increases as the gap-chord ratio of the aerofoils in the cascade arrangement is reduced.

2. Adjacent aerofoils in the cascade vibrate in antiphase. Hence alternate aerofoils have similar motions.

3. The frequency of the flutter is in general nearer to the torsional natural frequency than to the flexural natural frequency.

/4. ...

4. The variations in the critical flutter speed and frequency with stagger angle (at small angles of incidence) are relatively unimportant for stagger angles below 30°. At stagger angles greater than 35° constant amplitude flutter could not be maintained and the steady oscillatory motion was disturbed by pulsations probably originating from adjacent wakes.

5. Fair agreement between theory and experiment has been obtained. In view of the practical importance of this work, as for example in connection with the design of blading in axial compressors, it appears desirable to extend both the range of the experiments and the theory to high subsonic Mach numbers.

/Part 2 ...

PART 2

§1. Introduction

As far as is known to the author no theoretical papers (apart from reference 1) have been published on the flutter of aerofoils in cascade. It appears, however, in the light of the experimental results reported in Part 1, that the general theory of the flutter of aerofoils in cascade can be simplified, in a restricted sense, in view of the antiphase motions of adjacent aerofoils. The flutter characteristics can, however, only be calculated when the aerodynamic forces and moments on the oscillating aerofoil are known.

If we consider the air flow past a cascade of oscillating aerofoils in antiphase motion (see figure 15b) it can be seen that the flow about the mid lines, A'A' and B'B', between adjacent aerofoils, will be symmetrical for all positions of the aerofoils. The lines such as A'A' and B'B' are therefore streamlines of the motion and can thus be replaced by solid boundaries.

The flow around oscillating aerofoils in cascade at zero stagger is therefore equivalent to the tunnel wall interference on a single oscillating aerofoil, provided that adjacent aerofoils in the cascade have antiphase motions.

The three-dimensional problem of tunnel wall interference on an oscillating aerofoil has been investigated by W.P. Jones (reference 3). This theory is based on the vortex sheet method which replaces the aerofoil and its wake by suitable distributions of doublets, satisfying the following boundary conditions.

(a) The velocity at the trailing edge is finite.

(b) The normal induced velocity at the aerofoil, due to the doublet distributions, is equal to the normal components of the velocity of the aerofoil.

(c) The normal velocity at the walls is zero.

The calculation of the airloads, using this method, is very lengthy and unfortunately numerical values are quoted only for one height-chord ratio, which is considerably greater than the values of the gap-chord ratio of interest in this investigation.

/The ...

The corresponding problem in two-dimensions has been investigated by Reissner (reference 4) and Timman (reference 5), for incompressible flow and by Runyan and Watkins (reference 6) for compressible flow.

The essential details of the two-dimensional incompressible theory is presented below and the airload coefficients are given in a form such that rapid calculation is possible. Only a brief review of the essential results, quoted in the main in reference 4 and 5 is given. The method of presentation, however, has the advantage that a clear physical picture is obtained of the essential feature of the theory and simple results can be obtained for the values of certain airload coefficients as the gap-chord ratio approaches zero. As will be shown in Appendix 1 it is sufficient to calculate the variation of the stiffness derivatives with gap-chord ratio, if approximate values only of the flutter characteristics are required.

The extension of the incompressible theory to subsonic compressible flow is not considered in this paper. The theory developed in reference 6 is not in a form suitable for the evaluation of the airload coefficients. An important result obtained, however, in reference 6 is that the normal induced velocity at the aerofoil becomes infinite for certain values of $\tilde{\omega}$ s/c. This resonant condition corresponds to values of the frequency parameter given by

$$\tilde{\omega} = \frac{\pi\sqrt{1-M^2}}{\frac{s}{c}M}$$

where M is the freestream Mach number. According to this criterion the circular frequency ω is <u>infinite</u> for an incompressible fluid but it has finite values in a compressible fluid when M equals zero. These results are mentioned here since they may have an important bearing on the theory of cascade flutter applied to subsonic and supersonic compressible flow.

The theories outlined above only apply to the case of a cascade of aerofoils at zero stagger and zero incidence. The extension of the theory to other cases is being considered. The results discussed in Part 1 give the order of the variations involved, at least, for the case of stagger.

The calculation of the critical flutter speed and frequency is straightforward once the aerodynamic derivatives

/and ...

and the structural coefficients have been evaluated. The classical treatment of this problem in the case of flexure-torsion flutter is given in Appendix 1. It is important, however, not to overlook the fact that in reference 1 flutter with a single degree of freedom was experienced. This problem is also discussed below.

§2. The aerodynamic forces on an oscillating two-dimensional aerofoil in cascade in incompressible flow.

2.1. General theory

The axes of the fixed coordinates OX and OZ are taken as shown in figure 15. The origin of coordinates is at the midchord of aerofoil (O). The aerofoils, which are assumed to be infinitely thin, are oscillating with constant infinitesimal amplitude.

Let the components of velocity at (x, z) in the directions OX and OZ respectively be

$$V + u, \quad w$$

where the perturbation velocities u, w are small compared with the freestream velocity V. From the equations of continuity and motion for an inviscid and incompressible fluid, when second order terms are neglected, it can be shown that

$$\nabla^2 \phi = 0 \qquad \ldots\ldots\ldots 2.1$$

$$\nabla^2 \bar{\Phi} = 0 \qquad \ldots\ldots\ldots 2.2$$

where ϕ is the perturbation velocity potential, $\bar{\Phi} = \frac{p_o - p}{\rho}$ is the acceleration potential, p and ρ denote the pressure and density respectively and suffix o denotes the free stream value.

Bernoulli's equation for the unsteady motion of an incompressible fluid when second order velocity components are neglected becomes

$$\frac{\partial \phi}{\partial t} + Vu + \frac{p}{\rho} = \frac{p_o}{\rho} \qquad \ldots\ldots\ldots 2.3$$

which can be written

$$\bar{\Phi} = \left(\frac{\partial}{\partial t} + V \frac{\partial}{\partial x} \right) \phi \qquad \ldots\ldots\ldots 2.4$$

/If the ...

If the suffices + and - refer to the top and bottom surfaces of the aerofoils and their associated wakes then,

$$\left(\frac{\partial}{\partial t} + V\frac{\partial}{\partial x}\right)\left(\phi_+ - \phi_-\right) = \Phi_+ - \Phi_- \quad -\frac{c}{2} \leq x \leq \frac{c}{2} \quad \ldots\ldots 2.5$$

$$= 0 \qquad \frac{c}{2} \leq x \leq \infty \quad \ldots\ldots 2.6$$

since the pressure is continuous across the wake.

It is convenient in the further development of the theory to define $\gamma(x,t)$ as that part of the vorticity associated with the pressure loading and $(\gamma+\varepsilon)$ as the total vorticity, associated with the velocity difference, across the aerofoils. We will refer to $\gamma(x,t)$ as the bound vorticity and $\varepsilon(x,t)$ as the free vorticity.+ Using the above definitions it follows that

$$\Phi_+ - \Phi_- = V\gamma \qquad \ldots\ldots 2.7$$

and

$$u_+ - u_- = \frac{\partial}{\partial x}\left(\phi_+ - \phi_-\right) = \gamma+\varepsilon \qquad \ldots\ldots 2.8$$

The condition for finite loading at the trailing edges is satisfied by $\gamma(c/2)$ equals zero. It follows, from equation 2.8, that the condition for finite velocity at the trailing edges is that $\varepsilon(c/2)$ shall be finite. Since the aerofoils are infinitely thin the velocities around their leading edges will be infinite. Hence $\gamma(-c/2)$ will be infinite. By definition the values of $\varepsilon(-c/2)$ and $\varepsilon(\infty)$ are zero.

It follows that the total lift force, and the total pitching moment about the reference section, $x = x_f$, on each aerofoil at time t are respectively equal to

$$\Gamma(t) = \int_{-c/2}^{c/2} (\gamma+\varepsilon)\, dx \qquad \ldots\ldots 2.9$$

+ In two-dimensional steady aerofoil theory the free vorticity, as defined above, is of course everywhere equal to zero. In two-dimensional unsteady aerofoil theory the free vorticity over the aerofoil and its wake is due to the time variation of the bound vorticity.

$$-Z(t) = \rho V \int_{-c/2}^{c/2} \gamma \, dx \qquad \ldots\ldots\ldots 2.10$$

$$-M(t) = \rho V \int_{-c/2}^{c/2} \gamma (x - x_f) \, dx \qquad \ldots\ldots\ldots 2.11$$

If the aerofoils are in simple harmonic motion with circular frequency ω and similar motions are assumed for their wakes, and if we write all time variable quantities as $\gamma = \bar{\gamma} e^{i\omega t}$, $\varepsilon = \bar{\varepsilon} e^{i\omega t}$ etc. where $\bar{\gamma}$ and $\bar{\varepsilon}$ are complex quantities,+ then it follows from equations 2.6, 2.7 and 2.8 that

$$\phi_+ - \phi_- = \frac{iV}{\omega} \varepsilon \qquad \ldots\ldots\ldots 2.12$$

$$\gamma + \varepsilon = \frac{iV}{\omega} \frac{\partial \varepsilon}{\partial x} \qquad \ldots\ldots\ldots 2.13$$

and $$\gamma e^{i\omega x/V} = \frac{iV}{\omega} \frac{\partial}{\partial x} \left(\varepsilon \, e^{i\omega x/V} \right) \qquad \ldots\ldots\ldots 2.14$$

If we integrate equation 2.13 with respect to x between the limits $\frac{c}{2}$ and $-\frac{c}{2}$ then from equation 2.9

$$\Gamma(t) = \frac{iV}{\omega} \varepsilon\left(\frac{c}{2}, t\right) \qquad \ldots\ldots\ldots 2.15$$

Thus the instantaneous value of the circulation around each aerofoil is proportional to the free vorticity at the trailing edge.*

In addition the condition that the total vorticity is zero becomes

$$\int_{-c/2}^{\infty} (\gamma + \varepsilon) \, dx = 0 \qquad \ldots\ldots\ldots 2.16$$

/and ...

+ It is to be understood that only the real (or imaginary) part is finally taken.

* Or the rate of change of circulation around each aerofoil is equal to minus the product of the free stream velocity and the free vorticity at the trailing edge.

and since γ equals zero in the wakes

$$\int_{c/2}^{\infty} \varepsilon \, dx = - \int_{-c/2}^{c/2} (\gamma+\varepsilon) \, dx = - \Gamma(t) = - \frac{iV}{\omega} \varepsilon\left(\frac{c}{2}, t\right) \quad \ldots\ldots 2.17$$

by virtue of equation 2.15.

Thus the instantaneous value of the total free vorticity in the wake is equal in magnitude, but opposite in sign, to the instantaneous value of the circulation around the aerofoil.

Again if we use the condition that γ equals zero in the wakes, equation 2.14, when integrated with respect to x gives

$$\varepsilon(x,t) \, e^{i\omega x/V} = - \frac{i\omega}{V} \int_{-c/2}^{x} \gamma e^{i\omega x/V} dx \quad - \frac{c}{2} \leq x \leq \frac{c}{2}$$

$$= \varepsilon\left(\frac{c}{2}, t\right) e^{i\omega c/2V} \qquad \frac{c}{2} \leq x \leq \infty \qquad \ldots\ldots 2.18$$

Alternatively from equation 2.13

$$\varepsilon(x,t) = - \frac{i\omega}{V} \int_{-c/2}^{x} (\gamma+\varepsilon) \, dx$$

and $\qquad \ldots\ldots\ldots 2.19$

$$\varepsilon\left(\frac{c}{2}, t\right) = - \frac{i\omega}{V} \int_{-c/2}^{c/2} (\gamma+\varepsilon) \, dx$$

The amplitudes of the lift force and pitching moment become respectively on each aerofoil

$$- \frac{\bar{Z}}{\rho V c} = - \tfrac{1}{2} \int_{-1}^{1} \bar{\varepsilon}(x') dx' + \frac{i\bar{\varepsilon}(1)}{\tilde{\omega}}$$

$$- \frac{\bar{M}}{\rho V c^2} = - \frac{1}{4} \int_{-1}^{1} (x'-x_f') \, \bar{\varepsilon}(x') dx' + \frac{i\bar{\varepsilon}(1)}{2\tilde{\omega}} (1-x_f') - \frac{i}{2\tilde{\omega}} \int_{-1}^{1} \bar{\varepsilon}(x') dx'$$

$\ldots\ldots\ldots 2.20$

/where ...

where $\tilde{\omega} = \frac{\omega c}{V}$ denotes the non-dimensional frequency parameter and dashes denote values of x divided by $c/2$.

The discontinuities in ϕ across the surface of the aerofoils and their wakes can be represented by distributions of doublets of strengths equal to the local discontinuity. Thus

$$\phi(x,z,t) = \frac{1}{2\pi} \sum_{n=-\infty}^{\infty} \int_{-c/2}^{\infty} \tau(x_1, z_n, t) \int_{-\infty}^{x} \frac{\partial}{\partial z_n} \log r_n \, dx \, dx_1 \qquad \ldots\ldots\ldots 2.21$$

where $\tau = \gamma + \varepsilon$

$r_n^2 = (x-x_1)^2 + (z-z_n)^2$

and suffix n refers to the nth aerofoil from the axis OX.

When adjacent aerofoils are oscillating in antiphase with small amplitude $\tau(x_1, z_n, t) = (-1)^n \tau(x_1, z_o, t)$ and on differentiating equation 2.21 with respect to z and taking the limit as z tends to zero, we find that the normal induced velocity adjacent to the zeroth aerofoil[+] is

$$w(x,0,t) = \frac{1}{2s} \int_{-c/2}^{\infty} \frac{\tau(x_1,0,t)\, dx_1}{\sinh \frac{\pi}{s}(x-x_1)} \qquad \ldots\ldots\ldots 2.22$$

where s is the gap between adjacent blades.

But $w(x,0,t)$ must equal the normal velocity of the oscillating aerofoil. This can be written in terms of ζ, θ its displacement and rotation respectively about the reference axis as

$$w(x,t) = \left(\frac{\partial}{\partial t} + V\frac{\partial}{\partial x}\right)\left(\zeta + (x-x_f)\theta\right)$$

$$= V\left[\frac{i\tilde{\omega}\zeta'}{2} + \theta\left\{\frac{i\tilde{\omega}}{2}(x'-x_f') + 1\right\}\right]_{/On} \qquad \ldots\ldots 2.23$$

[+] The following relations are used

$$\int_{-\infty}^{x} \frac{\partial^2}{\partial z\, \partial z_n} \log r_n \, dx = \frac{x-x_1}{r_n^2}$$

$$z_n = ns$$

and $$\operatorname{cosech} y = \sum_{-\infty}^{\infty} (-1)^n \frac{y}{y^2 + n^2\pi^2} .$$

On equating equations 2.22 and 2.23 and dividing through by $e^{i\omega t}$ we obtain finally

$$\boxed{\bar{w}(x') \equiv \left[\frac{i\tilde{\omega}\bar{x}'}{2} + \bar{\theta}\left\{\frac{i\tilde{\omega}(x'-x_f')}{2} + 1\right\}\right] V = \frac{\lambda}{2\pi}\int_{-1}^{\infty} \frac{\bar{\tau}(x_1',0)\,dx_1'}{\sinh \lambda(x'-x_1')}}$$

.....2.24

where $\lambda = \frac{\pi c}{2s}$ and dashes denote quantities divided by c/2.

If we further write $\int_{-1}^{\infty} = \int_{1}^{\infty} + \int_{-1}^{1}$ and substitute from equation 2.18

$$\bar{w}(x) = \frac{\lambda}{2\pi}\int_{-1}^{1} \frac{\bar{\tau}(x_1)\,dx_1}{\sinh \lambda(x-x_1)} + \frac{\lambda\bar{\varepsilon}(1)}{2\pi}\int_{1}^{\infty} \frac{\exp\left(\frac{i\tilde{\omega}}{2}\left[1-x_1\right]\right)dx_1}{\sinh \lambda(x-x_1)}$$

.....2.25

where, for convenience, the dashes on x have been omitted.

Apart from changes in notation, equation 2.25 agrees with equation 68 of reference 4. On making the substitutions

$$\left.\begin{aligned} \tanh \lambda &= k \\ \tanh \lambda x &= k\alpha \\ \tanh \lambda x_1 &= k\alpha_1 \end{aligned}\right\}$$

.....2.26

equation 2.25 becomes

$$\frac{\bar{w}(\alpha)}{\sqrt{1-k^2\alpha^2}} = \frac{1}{2\pi}\int_{-1}^{1} \frac{\bar{\tau}(\alpha_1)d\alpha_1}{(\alpha-\alpha_1)\sqrt{1-k^2\alpha_1^2}} + \frac{\bar{\varepsilon}(1)}{2\pi}\int_{1}^{1/k} \frac{\exp\frac{i\tilde{\omega}}{2}\left(1 - \frac{\tanh^{-1} k\alpha_1}{\lambda}\right)d\alpha_1}{(\alpha-\alpha_1)\sqrt{1-k^2\alpha_1^2}}$$

.....2.27

The solution of the integral equation 2.27 can be obtained by the methods suggested in reference 4.[+] After a partial integration this becomes

---

+ If $g(x) = -\frac{1}{\pi}\int_{-1}^{1} \frac{f(\xi)d\xi}{(x-\xi)}$ then $f(x) = \frac{1}{\pi}\left(\frac{1-x}{1+x}\right)^{\frac{1}{2}}\int_{-1}^{1}\left(\frac{1+\xi}{1-\xi}\right)^{\frac{1}{2}} \frac{g(\xi)d\xi}{(x-\xi)}$

$$\frac{\bar{\tau}(\alpha)}{\sqrt{1-k^2\alpha^2}}\sqrt{\frac{1+\alpha}{1-\alpha}} = -\frac{2}{\pi}\int_{-1}^{1}\sqrt{\frac{1+\alpha_1}{1-\alpha_1}}\,\frac{\bar{w}(\alpha_1)\,d\alpha_1}{(\alpha-\alpha_1)\sqrt{1-k^2\alpha_1^2}}$$

$$+\frac{\bar{\varepsilon}(1)}{\pi}\int_{1}^{1/k}\sqrt{\frac{\alpha_1+1}{\alpha_1-1}}\,\frac{\exp\left(\frac{i\tilde{\omega}}{2}\left[1-\frac{\tanh^{-1}k\alpha_1}{\lambda}\right]\right)d\alpha_1}{(\alpha-\alpha_1)\sqrt{1-k^2\alpha_1^2}}$$

.....2.28

The value of $\bar{\varepsilon}(1)$ is obtained by integrating $\bar{\tau}(\alpha)$ with respect to α between the limits 1 and -1 and substituting from equation 2.19. After some rearrangement it can be shown that,

$$\bar{\varepsilon}(1) = -\frac{\frac{2k}{\pi\lambda}\int_{-1}^{1}\sqrt{\frac{1+\alpha_1}{1-\alpha_1}}\,\frac{\bar{w}(\alpha_1)}{\sqrt{1-k^2\alpha_1^2}}\left[\int_{-1}^{1}\sqrt{\frac{1-\alpha}{1+\alpha}}\,\frac{d\alpha}{(\alpha-\alpha_1)\sqrt{1-k^2\alpha^2}}\right]d\alpha_1}{\frac{2i}{\tilde{\omega}}-\frac{k}{\pi\lambda}\int_{1}^{1/k}\sqrt{\frac{\alpha_1+1}{\alpha_1-1}}\,\frac{\exp\left(\frac{i\tilde{\omega}}{2}\left[1-\frac{\tanh^{-1}k\alpha_1}{\lambda}\right]\right)}{\sqrt{1-k^2\alpha_1^2}}\left[\int_{-1}^{1}\sqrt{\frac{1-\alpha}{1+\alpha}}\,\frac{d\alpha}{(\alpha-\alpha_1)\sqrt{1-k^2\alpha^2}}\right]d\alpha_1}$$

.....2.29

The amplitudes of the lift force and pitching moment can be found directly from equations 2.19, 2.20, when $\bar{\tau}$ is substituted from equation 2.28 together with 2.29.

It is possible to simplify the above integrals for the case of small gap-chord ratios since when $s/c << 1$, $k \approx 1$, and λ is very large. The validity of the resulting expressions is limited however to values of the gap-chord ratio below 0.5.+

More general solutions to the above integrals can be obtained by transforming them in terms of Jacobean elliptic functions. The final expresseions obtained are in agreement with the solution obtained in a different way by Timman* (reference 5).

/Only ...

+ In particular in this region the airload coefficient

$$\bar{Z}_2 = \bar{Z}_3 = \frac{4\tilde{\omega}k}{\pi^2\lambda}K^2(k)$$

* Timman uses the method of conformal transformation.

It is an extension of Theodorsen's method for the two-dimensional isolated oscillating aerofoil.

Only the final expressions for the airload derivatives will be quoted here.

The airload coefficients will be expressed as follows

$$-\frac{\bar{Z}}{\pi\rho c V^2} = \bar{Z}_{12}\frac{\bar{h}\omega}{c} + \bar{Z}_{34}\bar{\theta}$$

$$-\frac{\bar{M}}{\pi\rho c^2 V^2} = \bar{M}_{12}\frac{\bar{h}\omega}{c} + \bar{M}_{34}\bar{\theta} \qquad \text{.....2.30}$$

where $\bar{Z}_{12} = \bar{Z}_1 + i\bar{Z}_2$

$\bar{M}_{12} = \bar{M}_1 + i\bar{M}_2$ etc.

and $\bar{M}$ now refers to the amplitude of the pitching moment about the mid-chord axis.

Then,

$$\bar{Z}_{12} = i\tilde{\omega}\frac{16s}{\pi c} Q_1 \left[\frac{1}{2} + (C-1)\left(1 - \frac{\pi^2 Q_1}{2kK^2}\right)\right] - \frac{16\tilde{\omega}^2 s^2 Q_2}{\pi^2 c^2} \qquad \text{.....2.31}$$

$$\bar{Z}_{34} = \frac{16s}{\pi c} Q_1 \left[\frac{1}{2} + (C-1)\left(1 - \frac{\pi^2 Q_1}{2kK^2}\right)\right] + i\tilde{\omega}\frac{32s^2}{\pi^2 c^2}\left[Q_2 + \frac{Q_1 Q_3}{2kK^2}(C-1)\pi^2\right]$$

.....2.32

$$\bar{M}_{12} = -i\tilde{\omega}\frac{32s^2}{\pi^2 c^2} Q_3 \left[\frac{1}{2} + (C-1)\left(1 - \frac{\pi^2 Q_1}{2kK^2}\right)\right] \qquad \text{.....2.33}$$

$$\bar{M}_{34} = -\frac{32s^2}{\pi^2 c^2} Q_3 \left[\frac{1}{2} + (C-1)\left(1 - \frac{\pi^2 Q_1}{2kK^2}\right)\right] \qquad \text{.....2.34}$$

$$- \tilde{\omega}^2 \frac{32s^4}{\pi^4 c^4} Q_4 - i\tilde{\omega}\frac{32s^3}{\pi k K^2 c^3} Q_3^2 (C-1)$$

where the generalised Theodorsen function[+] $C\left(\tilde{\omega}, \frac{s}{c}\right) \equiv A - iB =$

+ Timman (reference 5) expresses the airload coefficients in terms of a generalised Küssner function $T\left(\frac{\tilde{\omega}s}{2\pi c}, k\right) \equiv 2C-1$. Equations 2.31 to 2.40 are not identical with the expressions quoted in reference 5, since a number of minor errors exist in the printed paper.

$$\left[ibF\left(\tfrac{1}{2}, ib-\tfrac{1}{2}; ib; \frac{1}{\beta^2}\right) - \frac{(ib+\frac{1}{2})^2}{(ib+1)\beta^2} F\left(\tfrac{1}{2}, ib+\tfrac{3}{2}; ib+2; \frac{1}{\beta^2}\right) + \right.$$

$$\left. \frac{1}{\beta}\left(\frac{2E}{Kk'^2} - 1 - i\frac{4kb}{k'^2}\right) F\left(\tfrac{1}{2}, ib+\tfrac{1}{2}; ib+1; \frac{1}{\beta^2}\right)\right] \quad \ldots\ldots\ldots 2.35$$

$$\left[ibF\left(\tfrac{1}{2}, ib-\tfrac{1}{2}; ib; \frac{1}{\beta^2}\right) - \frac{(ib+\frac{1}{2})^2}{(ib+1)\beta^2} F\left(\tfrac{1}{2}, ib+\tfrac{3}{2}; ib+2; \frac{1}{\beta^2}\right) + \right.$$

$$\left. \frac{1}{\beta}\left(\frac{2E}{Kk'^2} - 1 + i\frac{4kb}{k'^2}\right) F\left(\tfrac{1}{2}, ib+\tfrac{1}{2}; ib+1; \frac{1}{\beta^2}\right)\right]$$

where $F\left(\tfrac{1}{2}, ib-\tfrac{1}{2}; ib; \frac{1}{\beta^2}\right)$ etc. are hypergeometric functions

$$b = \frac{\tilde{\omega} s}{2\pi c}$$

and $$\beta = e^{\pi c/s}.$$

It reduces to the standard value

$$C = \frac{i H_1^{(2)}\left(\frac{\tilde{\omega}}{2}\right)}{i H_1^{(2)}\left(\frac{\tilde{\omega}}{2}\right) - H_o^{(2)}\left(\frac{\tilde{\omega}}{2}\right)} \quad \ldots\ldots\ldots 2.36$$

when $\frac{s}{c}$ tends to infinity.

In equations 2.31 to 2.35 inclusive,+

$$Q_1 = \sum_{n=0}^{\infty} \frac{q^{n+\frac{1}{2}}(1+q^{2n+1})}{(1-q^{2n+1})^2} \quad \ldots\ldots\ldots 2.37$$

$$Q_2 = \sum_{n=0}^{\infty} \frac{q^{2n+1}(1+q^{2n+1})}{(2n+1)(1-q^{2n+1})^3} \quad \ldots\ldots\ldots 2.38$$

$$Q_3 = \sum_{n=1}^{\infty} \gamma_n \frac{q^n(1+q^{2n})}{(1-q^{2n})} \quad \ldots\ldots\ldots 2.39$$

$$Q_4 = \sum_{n=1}^{\infty} \gamma_n^2 \frac{q^{2n}(1+q^{2n})}{n(1-q^{2n})} \quad \ldots\ldots\ldots 2.40$$

+ The functions Q_1 to Q_4 used in this report are not identical with the functions which are sometimes used in connection with the theta function.

$$\gamma_n = n \sum_{m=0}^{m=n-1} \frac{1}{(2m+1)(2n-2m-1)(1-q^{2m+1})(1-q^{2n-2m-1})}$$

$$+ 2n \sum_{m=0}^{\infty} \frac{q^{2m+1}}{(2m+1)(2n+2m+1)(1-q^{2m+1})(1-q^{2n+2m+1})} \quad \ldots\ldots 2.41$$

$$q = e^{-\pi K'/K} \qquad 0 \leq q \leq 1 \qquad \ldots\ldots\ldots 2.42$$

$$k = \tanh\left(\frac{\pi c}{2s}\right) \; ; \quad k^2 + k'^2 = 1$$

$K(k)$; $K'(k)$ are the complete elliptic integrals of the first kind of order k, and $E(k)$ is the complete elliptic integral of the second kind of order k.

§2.2. Approximate value of C for small values of the gap-chord ratio

The hypergeometric functions in equation 2.35 can be expanded in the following power series,

$$F(a,b;c;z) = 1 + \frac{a.b}{1.c} z + \frac{a(a+1)b(b+1)}{1.2.c(c+1)} z^2 \quad \text{when} \quad |z| < 1.$$

For small values of the gap-chord ratio $\frac{1}{\beta^2} << 1$ and then, for most practical applications, we need only the first two terms of the above series. Also in evaluating $C(\tilde{\omega}, \frac{s}{c})$ from equation 2.35 it is noted that $E(k)$ and k^2 tend to unity and k'^2 to zero as the gap-chord ratio tends to zero.+ If we use these approximations we find that in the range $0 < \frac{s}{c} < 1$ equation 2.35 reduces to

$$A = \frac{\left(E - \frac{Kk'^2}{2}\right)^2 + 8b^2K^2}{\left(E - \frac{Kk'^2}{2}\right)^2 + 16b^2K^2} \qquad \ldots\ldots\ldots 2.43$$

and

$$B = \frac{2bK\left(E - \frac{Kk'^2}{2}\right)}{\left(E - \frac{Kk'^2}{2}\right)^2 + 16b^2K^2} \qquad \ldots\ldots\ldots 2.44$$

/For very ...

+ For small values of s/c $K(k) \approx \log_e \frac{4}{k'}$ and $K'(k) \approx \frac{\pi}{2}$.

Hence $q \equiv e^{-\frac{\pi K'}{K}} \approx e^{-\frac{\pi^2}{2(\frac{\pi c}{2s} + \log_e 2)}}$

For very small values of the gap-chord ratio

$$A = \frac{1 + \frac{\tilde{\omega}^2}{2}\left(1 + \frac{2s}{\pi c}\log_e 2\right)^2}{1 + \tilde{\omega}^2\left(1 + \frac{2s}{\pi c}\log_e 2\right)^2} \qquad \ldots\ldots\ldots 2.45$$

and

$$B = \frac{\frac{\tilde{\omega}}{2}\left(1 + \frac{2s}{\pi c}\log_e 2\right)}{1 + \tilde{\omega}^2\left(1 + \frac{2s}{\pi c}\log_e 2\right)^2} \qquad \ldots\ldots\ldots 2.46$$

The asymptotic values of their derivatives with respect to the gap-chord ratio are

$$\left[\frac{\partial A}{\partial s/c}\right]_{s/c\to 0} = -\frac{\frac{2}{\pi}\tilde{\omega}^2 \log_e 2}{(1 + \tilde{\omega}^2)^2} \qquad \ldots\ldots\ldots 2.47$$

$$\left[\frac{\partial B}{\partial s/c}\right]_{s/c\to 0} = +\frac{\frac{\tilde{\omega}}{\pi}(1-\tilde{\omega}^2)\log_e 2}{(1 + \tilde{\omega}^2)^2} \qquad \ldots\ldots\ldots 2.48$$

The functions A and B are plotted in figure 16 for certain values of the frequency parameter $\tilde{\omega}$.

§2.3. The evaluation of the functions Q_1, Q_2, Q_3, Q_4.

The functions Q_1, Q_2, Q_3 and Q_4 are determined from the infinite series in the function q (see equation 2.42). Now for small values of the gap-chord ratio q varies from 0.1 to 1.0 and in this range the series are not rapidly convergent. They have been evaluated, by direct summation, to three decimal places and the results are given in table 3 and figures 17 and 18.

§2.4. The two-dimensional aerodynamic derivatives

If the lift and pitching moment are written respectively

$$\bar{Z} = Z_z z + Z_{\dot{z}}\dot{z} + Z_{\ddot{z}}\ddot{z} + Z_\theta\theta + Z_{\dot{\theta}}\dot{\theta} + Z_{\ddot{\theta}}\ddot{\theta} \qquad \ldots\ldots\ldots 2.49$$

$$\bar{M} = M_z z + M_{\dot{z}}\dot{z} + M_{\ddot{z}}\ddot{z} + M_\theta\theta + M_{\dot{\theta}}\dot{\theta} + M_{\ddot{\theta}}\ddot{\theta}$$

/then from ...

then from equations 2.30,

$$\bar{Z}_{12} = -\frac{Z_z}{\pi\rho V^2} - \frac{i\tilde{\omega}Z_{\dot{z}}}{\pi\rho cV} + \frac{\tilde{\omega}^2 Z_{\ddot{z}}}{\pi\rho c^2}$$

$$\bar{Z}_{34} = -\frac{Z_\theta}{\pi\rho cV^2} - \frac{i\tilde{\omega}Z_{\dot{\theta}}}{\pi\rho c^2 V} + \frac{\tilde{\omega}^2 Z_{\ddot{\theta}}}{\pi\rho c^3}$$

$$\bar{M}_{12} = -\frac{M_z}{\pi\rho cV^2} - \frac{i\tilde{\omega}M_{\dot{z}}}{\pi\rho c^2 V} + \frac{\tilde{\omega}^2 M_{\ddot{z}}}{\pi\rho c^3} \qquad \text{.....2.50}$$

$$\bar{M}_{34} = -\frac{M_\theta}{\pi\rho c^2 V^2} - \frac{i\tilde{\omega}M_{\dot{\theta}}}{\pi\rho c^3 V} + \frac{\tilde{\omega}^2 M_{\ddot{\theta}}}{\pi\rho c^4}$$

The values of the aerodynamic derivatives referred to the <u>mid-chord axis</u> are, from equations 2.31 to 2.34 inclusive,

$$\ell_z = -\frac{Z_z}{\rho V^2} = 0$$

$$\ell_{\dot{z}} = -\frac{Z_{\dot{z}}}{\rho cV} = 16\frac{s}{c}Q_1\left[\tfrac{1}{2} + (A-1)\left(1 - \frac{\pi^2 Q_1}{2kK^2}\right)\right]$$

$$\ell_{\ddot{z}} = -\frac{Z_{\ddot{z}}}{\rho c^2} = \frac{16s^2}{\pi c^2}\left[Q_2 - Q_1\frac{B}{\tilde{\omega}}\frac{\pi c}{s}\left(1 - \frac{\pi^2 Q_1}{2kK^2}\right)\right]$$

$$\ell_\theta = -\frac{Z_\theta}{\rho cV^2} = 16\frac{s}{c}Q_1\left[\tfrac{1}{2} + (A-1)\left(1 - \frac{\pi^2 Q_1}{2kK^2}\right)\right] \qquad \text{.....2.51}$$

$$\ell_{\dot{\theta}} = -\frac{Z_{\dot{\theta}}}{\rho c^2 V} = \frac{32s^2}{\pi c^2}\left[Q_2 + (A-1)\frac{\pi^2 Q_1 Q_3}{2kK^2}\right] - 16\frac{s}{c}Q_1\frac{B}{\tilde{\omega}}\left(1 - \frac{\pi^2 Q_1}{2kK^2}\right)$$

$$\ell_{\ddot{\theta}} = -\frac{Z_{\ddot{\theta}}}{\rho c^3} = -\frac{32s^2}{\pi c^2}\left(\frac{\pi^2 Q_1 Q_3 B}{2kK^2\tilde{\omega}}\right)$$

$$m_z = -\frac{M_z}{\rho cV^2} = 0$$

$$m_{\dot{z}} = -\frac{M_{\dot{z}}}{\rho c^2 V} = -\frac{32s^2}{\pi c^2}Q_3\left[\tfrac{1}{2} + (A-1)\left(1 - \frac{\pi^2 Q_1}{2kK^2}\right)\right]$$

$$m_{\ddot{z}} = -\frac{M_{\ddot{z}}}{\rho c^3} = \frac{32s^2}{\pi c^2}Q_3\frac{B}{\tilde{\omega}}\left(1 - \frac{\pi^2 Q_1}{2kK^2}\right)$$

$$m_\theta = -\frac{M_\theta}{\rho c^2 V^2} = -\frac{32s^2}{\pi c^2}Q_3\left[\tfrac{1}{2} + (A-1)\left(1 - \frac{\pi^2 Q_1}{2kK^2}\right)\right]$$

/$m_{\dot{\theta}}$ = ...

$$m_{\dot\theta} = -\frac{M_{\dot\theta}}{\rho c^3 V} = -\frac{32s^3}{kK^2c^3}Q_3^2\,(A-1) + \frac{32s^2}{\pi c^2}Q_3\left(1 - \frac{\pi^2 Q_1}{2kK^2}\right)\frac{B}{\tilde\omega}$$

$$m_{\ddot\theta} = -\frac{M_{\ddot\theta}}{\rho c^4} = \frac{32s^4}{\pi^3 c^4}Q_4 + \frac{32s^3 Q_3^2\, B}{k\,K^2 c^3\,\tilde\omega}$$

The variations of the derivatives $\ell_{\dot z}$, ℓ_θ, $m_{\dot z}$, m_θ with gap-chord ratio are shown in figure 19.

If the reference axis is taken hc forward of the mid-chord position and the corresponding values of the derivatives are denoted by $\bar\ell_z$, $\bar m_z$ etc. then the transformation formulae are

$$\bar\ell_z = \ell_z\;;\quad \bar\ell_{\dot z} = \ell_{\dot z}\;;\quad \bar\ell_{\ddot z} = \ell_{\ddot z}$$

$$\bar\ell_\theta = \ell_\theta + h\ell_z\;;\quad \bar\ell_{\dot\theta} = \ell_{\dot\theta} + h\ell_{\dot z}\;;\quad \bar\ell_{\ddot\theta} = \ell_{\ddot\theta} + h\ell_{\ddot z}$$

$$\bar m_z = m_z + h\ell_z\;;\quad \bar m_{\dot z} = m_{\dot z} + h\ell_{\dot z}\;;\quad \bar m_{\ddot z} = m_{\ddot z} + h\ell_{\ddot z}$$

$$\bar m_\theta = m_\theta + h(m_z + \ell_\theta) + h^2\ell_z \qquad \text{.....2.52}$$

$$\bar m_{\dot\theta} = m_{\dot\theta} + h(m_{\dot z} + \ell_{\dot\theta}) + h^2\ell_{\dot z}$$

$$\bar m_{\ddot\theta} = m_{\ddot\theta} + h(m_{\ddot z} + \ell_{\ddot\theta}) + h^2\ell_{\ddot z}\;.$$

§2.5. The three-dimensional flutter derivatives

Although the theory derived above can be logically extended to aerofoils of finite aspect ratio in cascade the added complications[+] appear unnecessary in this preliminary estimation of the magnitude of the cascade effect. It will be assumed therefore that the lift loading at all spanwise positions on the aerofoil will be similar and directly proportional to its local displacement and rotation. The aerofoils will be assumed to be of constant chord.

If the normal displacement of the zeroth aerofoil is given by

$$\zeta = \ell\phi\, f(\eta) + (x - x_f)\theta\, F(\eta) \qquad \text{.....2.53}$$

where $\eta = y/\ell$

= the distance from the root to the reference section.

+ Since the wake plays a minor role in the determination of the airloads on an aerofoil in a cascade of small gap-chord ratio, it might be inferred that the effect of the tip vortex would not be very marked.

$f(\eta)$ and $F(\eta)$ = the flexural and torsional modes of vibration

ϕ, θ = the angular displacements in flexure and torsion at the reference section relative to the root.

x_f = the chordwise position of the reference axis in the reference section,

then the amplitudes of the flexural and torsional moments about the root section can be expressed by,

$$-\frac{\bar{L}}{\rho V^2 \ell^3} = \bar{L}_{12}\,\phi + \bar{L}_{34}\,\vartheta$$

$$-\frac{\bar{M}}{\rho V^2 \ell^2 c} = \bar{M}_{12}\,\phi + \bar{M}_{34}\,\vartheta \qquad \text{.....2.54}$$

where $\vartheta = \frac{\theta c}{\ell}$.

The aerodynamic derivatives are derived from

$$\begin{aligned}
\bar{L}_{12} &= c_1 + i\tilde{\omega}\, b_1 - \tilde{\omega}^2\, a_1 \\
\bar{L}_{34} &= c_3 + i\tilde{\omega}\, b_3 - \tilde{\omega}^2\, g_1 \\
\bar{M}_{12} &= k_1 + i\tilde{\omega}\, j_1 - \tilde{\omega}^2\, a_3 \\
\bar{M}_{34} &= k_3 + i\tilde{\omega}\, j_3 - \tilde{\omega}^2\, g_3
\end{aligned} \qquad \text{.....2.55}$$

where,[+]

$$a_1 = \bar{\ell}_{\ddot{z}} \int_0^1 f^2 d\eta \qquad b_1 = \bar{\ell}_{\dot{z}} \int_0^1 f^2 d\eta$$

$$c_1 = \bar{\ell}_{z} \int_0^1 f^2 d\eta \qquad g_1 = \bar{\ell}_{\ddot{\theta}} \int_0^1 fF\, d\eta$$

$$j_1 = \bar{\ell}_{\dot{\theta}} \int_0^1 fF\, d\eta \qquad k_1 = \bar{\ell}_{\dot{\theta}} \int_0^1 fF\, d\eta$$

$$a_3 = \bar{m}_{\ddot{z}} \int_0^1 fF\, d\eta \qquad b_3 = \bar{m}_{\dot{z}} \int_0^1 fF\, d\eta \qquad \text{...2.56}$$

$$c_3 = \bar{m}_{z} \int_0^1 fF\, d\eta \qquad g_3 = \bar{m}_{\ddot{\theta}} \int_0^1 F^2 d\eta$$

/j_3 = ...

+ The derivatives are written as $\bar{\ell}_{\ddot{z}}$ ... , $\bar{m}_{\ddot{\theta}}$ ... , to show that two-dimensional values are being used. It is more usual to use the notation $\lambda_{\ddot{\phi}}$ ..., $\mu_{\ddot{\theta}}$ ... , for these same derivatives when three-dimensional values are being used.

$$j_3 = \bar{m}_\theta \int_0^1 F^2 d\eta \qquad k_3 = \bar{m}_\theta \int_0^1 F^2 d\eta$$

and the reference axis is taken at hc forward of the mid-chord position.

The complete coefficients a_1 , b_1 etc. must include both the aerodynamic and the structural components.

§3. Flutter with a single degree of freedom

Uncoupled flexural or torsional oscillations can occur when the coupling terms G_1 , J_1 , K_1 and A_3 , B_3 , C_3 (see equations A1.1) are zero.

The equations of motion for uncoupled flexural and torsional oscillations are respectively,

$$\begin{aligned} A_1 \ddot{\phi} + B_1 \dot{\phi} + C_1 \phi &= 0 \\ G_3 \ddot{\theta} + J_3 \dot{\theta} + K_3 \theta &= 0 \end{aligned} \qquad \text{.....3.1}$$

where ϕ is the flexural coordinate and θ is the torsional coordinate.

Flutter can therefore occur in the flexural and torsional modes, when respectively B_1 and J_3 are zero. In the notation of §2 this would require $\bar{l}_z$ or $\bar{m}_\theta$ to be zero.

Hence for flutter with a single degree of freedom either

$$g_1 = 0 \; ; \quad j_1 = 0 \; ; \quad k_1 = 0 \; ; \quad b_1 = 0$$

or

$$a_3 = 0 \; ; \quad b_3 = 0 \; ; \quad c_3 = 0 \; ; \quad j_3 = 0 \qquad \text{.....3.2}$$

It can be shown from an analysis of the terms given in equations 2.51 and 2.56 that these conditions cannot be satisfied. It is probable, however, that for oscillations having finite amplitude, the values of the aerodynamic derivatives will be reduced below those stated in equations 2.51 (see Appendix 2) and more exact analysis may show that under certain conditions equations 3.2 can be satisfied.

/Table 3 ...

TABLE 3

q	Q_1	Q_2	Q_3	Q_4
0	0	0	0	0
0.05	0.272	0.061	0.061	0.003
0.1	0.465	0.151	0.151	0.018
0.2	0.953	0.472	0.472	0.133
0.3	1.702	1.148	1.148	0.613
0.4	2.939	2.623	2.623	2.481
0.5	-	-	-	-
0.6	9.456	15.209	15.209	47.128

Note.

1. Tabulated values have been obtained by term by term summation.

2. Five decimal places have been used throughout.

3. The following values of γ_n were calculated and were used in the evaluation of Q_3 and Q_4.

q	γ_1	γ_2	γ_3	γ_4	γ_5	γ_6
0	1.0	1.333	1.533	1.676	1.787	1.878
0.05	1.143	1.446	1.642	-	-	-
0.1	1.309	1.572	1.763	1.903	2.013	2.103
0.2	1.732	1.882	2.055	2.191	2.299	2.388
0.3	2.338	2.307	2.444	2.570	2.675	2.762
0.4	3.262	2.927	2.990	3.094	3.191	3.275
0.5	-	-	-	-	-	-
0.6	7.571	5.616	5.192	5.104	5.120	5.168

q	γ_7	γ_8	γ_9	γ_{10}	γ_{11}	γ_{12}
0	1.955	2.022	2.081	-	-	-
0.1	2.179	2.246	2.304	-	-	-
0.2	2.463	2.538	2.588	-	-	-
0.3	2.837	2.903	2.961	-	-	-
0.4	3.349	3.413	3.470	3.522	3.597	3.611
0.5	-	-	-	-	-	-
0.6	5.223	5.278	5.330	5.379	5.422	5.464

q	γ_{13}	γ_{14}	γ_{15}	γ_{16}	γ_{17}	γ_{18}
0.4	-	-	-	-	-	-
0.5	-	-	-	-	-	-
0.6	5.503	5.538	5.572	5.603	5.633	5.661

Table 3 - Contd.

q	γ_{19}	γ_{20}	γ_{21}	γ_{22}
0.4	-	-	-	-
0.5	-	-	-	-
0.6	5.687	5.712	5.736	5.759

$$Q_1 = q^{\frac{1}{2}} \sum_{n=0}^{\infty} \frac{q^n (1 + q^{2n+1})}{(1 - q^{2n+1})^2} \qquad Q_3 = \sum_{n=1}^{\infty} \gamma_n \frac{q^n (1 + q^{2n})}{(1 - q^{2n})}$$

$$Q_2 = \sum_{n=0}^{\infty} \frac{q^{2n+1} (1 + q^{2n+1})}{(2n+1)(1 - q^{2n+1})^3} \qquad Q_4 = \sum_{n=1}^{\infty} \gamma_n^2 \frac{q^{2n} (1 + q^{2n})}{n(1 - q^{2n})}$$

$$\gamma_n = n \sum_{m=0}^{m=n-1} \frac{1}{(2m+1)(2n-2m-1)(1-q^{2m+1})(1-q^{2n-2m-1})}$$

$$+ 2n \sum_{m=0}^{\infty} \frac{q^{2m+1}}{(2m+1)(2n+2m+1)(1-q^{2m+1})(1-q^{2n+2m+1})}$$

REFERENCES

No.	Author	Title etc.
1.	Ch. Bellenot and J. Lalive d'Epinay	Self induced vibrations of turbo-machine blades Brown Boveri Review Vol.37, pp.368-376. 1950.
2.	W.J. Duncan	The fundamentals of flutter. 1951 A.R.C. R. and M. 2417,
3.	W. Pritchard Jones	Wind tunnel interference effects on the values of experimentally determined derivative coefficients for oscillating aerofoils. 1943. A.R.C. R. and M. 1912.
4.	E. Reissner	Boundary value problems in aero-dynamics of lifting surfaces in non-uniform motion. Bulletin of the American Math.Soc. Vol. 55, 1949, pp.825-850.

/5. ...

No.	Author	Title etc.
5.	R. Timman	The aerodynamic forces on an oscillating aerofoil between two parallel walls. Applied Scientific Research Vol.A3 No. 1, 1951, pp.31-57.
6.	H.L. Runyan and C.E. Watkins	Considerations of the effect of wind tunnel walls on oscillating air forces for two-dimensional subsonic compressible flow. 1951. N.A.C.A. T.N. 2552.
7.	W. Pritchard Jones	Summary of formulae and notations used in two-dimensional derivative theory. 1942. A.R.C. R. and M. 1958.
8.	H. Lamb	Hydrodynamics 6th edition 1932. pp. 190-192 (C.U.P.)

/Appendix 1 ...

APPENDIX 1

The calculation of the critical flutter speed and frequency for coupled flexure-torsion flutter.

A brief account of the essential features of flutter theory are given, for completeness, below. A more detailed account can be found, for example, in reference 2.

The equations of motion describing the vibration of a rectangular cantilevered aerofoil in cascade are (reference 2)

$$A_1\ddot{\phi} + B_1\dot{\phi} + C_1\phi + G_1\ddot{\theta} + J_1\dot{\theta} + K_1\theta = 0$$

$$A_3\ddot{\phi} + B_3\dot{\phi} + C_3\phi + G_3\ddot{\theta} + J_3\dot{\theta} + K_3\theta = 0 \qquad \ldots\ldots\ldots\text{A1.1}$$

where ϕ is the flexural coordinate (the downward displacement z of the extremity of the flexural axis at the tip section divided by the span ℓ)

and θ is the torsional coordinate (the twist at the tip section - positive when the leading edge rises and the trailing edge falls).

If $f(\eta)$ and $F(\eta)$ are the flexural and torsional modes respectively then the downward displacement at the point (x,y) is

$$z = \phi\ell f(\eta) + \theta c\,(\xi-\bar{\xi})F(\eta) \ldots \qquad \ldots\ldots\ldots\text{A1.2}$$

where $\eta = y/\ell$

$\xi = x/c$

$\bar{\xi}\,c$ is the distance of the flexural axis from the leading edge

ℓ = span (root to tip)

c = chord

and x, y, z are rectangular cartesian coordinates having their origin at the leading edge of the root section (see figure 20).

The boundary conditions are that+

$$\begin{aligned} f(0) &= F(0) = 0 \\ f(1) &= F(1) = 1 \\ f'(0) &= F'(1) = 0 \\ f''(1) &= f'''(1) = 0 \end{aligned} \qquad \ldots\ldots\ldots\text{A1.3}$$

/If ...

+ Good approximations to the flexural and torsional modes are $f(\eta) = \eta^2$ and $F(\eta) = \eta$.

If, for a harmonic motion, $\phi = \bar{\phi}\, e^{i\omega t}$ and $\theta = \bar{\theta}\, e^{i\omega t}$, where $\bar{\phi}$ and $\bar{\theta}$ are the amplitudes and ω is the circular frequency, then from equations A1.1, when $\bar{\phi}$ and $\bar{\theta}$ have been eliminated,

$$q_o\,\omega^4 - iq_1\omega^3 - q_2\omega^2 + iq_3\omega + q_4 = 0 \qquad \text{.....A1.4}$$

which has the solutions

$$\omega^2 = q_3 / q_1 \qquad \text{.....A1.5}$$

and

$$q_1\, q_2\, q_3 - q_o\, q_3^2 - q_1^2\, q_4 = 0 \qquad \text{.....A1.6}$$

where

$$q_o = \begin{vmatrix} A_1 & G_1 \\ A_3 & G_3 \end{vmatrix}$$

$$q_1 = \begin{vmatrix} A_1 & J_1 \\ A_3 & J_3 \end{vmatrix} + \begin{vmatrix} B_1 & G_1 \\ B_3 & G_3 \end{vmatrix}$$

$$q_2 = \begin{vmatrix} A_1 & K_1 \\ A_3 & K_3 \end{vmatrix} + \begin{vmatrix} B_1 & J_1 \\ B_3 & J_3 \end{vmatrix} + \begin{vmatrix} C_1 & G_1 \\ C_3 & G_3 \end{vmatrix} \qquad \text{.....A1.7}$$

$$q_3 = \begin{vmatrix} B_1 & K_1 \\ B_3 & K_3 \end{vmatrix} + \begin{vmatrix} C_1 & J_1 \\ C_3 & J_3 \end{vmatrix}$$

$$q_4 = \begin{vmatrix} C_1 & K_1 \\ C_3 & K_3 \end{vmatrix}$$

If
- m = mass per unit length of span
- $\bar{\xi}\, c$ = distance of the centre of gravity from the leading edge
- $mc^2\kappa^2$ = the polar moment of inertia per unit length about the leading edge
- ℓ_ϕ = flexural stiffness
- m_θ = torsional stiffness
- ρ = density
- V = wind speed

the coefficients A_1, B_1 etc. can be expressed in the following non-dimensional forms,+

$$a_1 = \frac{A_1}{\rho c^2 \ell^3} = \lambda \ddot{\phi} \int_o^1 f^2 d\eta + \frac{1}{\rho c^2} \int_o^1 m\, f^2 d\eta \qquad \text{.....A1.8}$$

/b_1 = ...

+ It should be noted that some of the coefficients are different from those used in reference 2.

$$b_1 = \frac{B_1}{\rho V c \ell^3} = \lambda_{\dot{\phi}} \int_0^1 f^2 d\eta \qquad \text{.....A1.9}$$

$$c_1 = \frac{C_1}{\rho V^2 \ell^3} = \lambda_{\phi} \int_0^1 f^2 d\eta + \frac{\ell_{\phi}}{\rho V^2 \ell^3} \qquad \text{.....A1.10}$$

$$g_1 = \frac{G_1}{\rho \ell^2 c^3} = \lambda_{\ddot{\theta}} \int_0^1 fF\, d\eta + \frac{1}{\rho c^2} \int_0^1 (\bar{\xi}-\bar{\bar{\xi}}) m\, fF\, d\eta \qquad \text{.....A1.11}$$

$$j_1 = \frac{J_1}{\rho V c^2 \ell^2} = \lambda_{\dot{\theta}} \int_0^1 fF\, d\eta \qquad \text{.....A1.12}$$

$$k_1 = \frac{K_1}{\rho V^2 \ell^2 c} = \lambda_{\theta} \int_0^1 fF\, d\eta \qquad \text{.....A1.13}$$

$$a_3 = \frac{A_3}{\rho \ell^2 c^3} = \mu_{\ddot{\phi}} \int_0^1 fF\, d\eta + \frac{1}{\rho c^2} \int_0^1 (\bar{\xi}-\bar{\bar{\xi}}) m\, fF\, d\eta \qquad \text{.....A1.14}$$

$$b_3 = \frac{B_3}{\rho V \ell^2 c^2} = \mu_{\dot{\phi}} \int_0^1 fF\, d\eta \qquad \text{.....A1.15}$$

$$c_3 = \frac{C_3}{\rho V^2 \ell^2 c} = \mu_{\phi} \int_0^1 fF\, d\eta \qquad \text{.....A1.16}$$

$$g_3 = \frac{G_3}{\rho \ell c^4} = \mu_{\ddot{\theta}} \int_0^1 F^2 d\eta + \frac{1}{\rho c^2} \int_0^1 (\bar{\bar{\xi}}^2 - 2\bar{\bar{\xi}}\,\bar{\xi} + \bar{k}^2) m\, F^2 d\eta \qquad \text{..A1.17}$$

$$j_3 = \frac{J_3}{\rho V \ell c^3} = \mu_{\dot{\theta}} \int_0^1 F^2 d\eta \qquad \text{.....A1.18}$$

$$k_3 = \frac{K_3}{\rho V^2 \ell c^2} = \mu_{\theta} \int_0^1 F^2 d\eta + \frac{m_{\theta}}{\rho V^2 \ell c^2} \qquad \text{.....A1.19}$$

In the above formulae $\lambda_{\ddot{\phi}}$ etc. represent the overall aerodynamic flexural derivatives and $\mu_{\ddot{\phi}}$ etc. represent the overall aerodynamic torsional derivatives. The reference axis is taken as the flexural axis of the reference section+. The

/effect ...

+ The aerodynamic derivatives are functions of the plan form, aerofoil section and the frequency parameter ω. For preliminary calculations of the flutter speed and frequency sufficient accuracy is obtained if two-dimensional derivatives appropriate to the required frequency parameter are used.

effect of hysteresis or structural damping has been neglected.

If the non-dimensional coefficients above are substituted into equation A1.5 and A1.6

$$\bar{q}_1\,\bar{q}_2\,\bar{q}_3 - \bar{q}_o\,\bar{q}_3^2 - \bar{q}_1^2\,\bar{q}_4 = 0 \qquad \text{.....A1.20}$$

and

$$\tilde{\omega} = \frac{\omega c}{V} = \sqrt{\frac{\bar{q}_3}{\bar{q}_1}} \qquad \text{.....A1.21}$$

where

$$\bar{q}_o = \begin{vmatrix} a_1 & g_1 \\ a_3 & g_3 \end{vmatrix}$$

$$\bar{q}_1 = \begin{vmatrix} a_1 & j_1 \\ a_3 & j_3 \end{vmatrix} + \begin{vmatrix} b_1 & g_1 \\ b_3 & g_3 \end{vmatrix}$$

$$\bar{q}_2 = \begin{vmatrix} a_1 & k_1 \\ a_3 & k_3 \end{vmatrix} + \begin{vmatrix} b_1 & j_1 \\ b_3 & j_3 \end{vmatrix} + \begin{vmatrix} c_1 & g_1 \\ c_3 & g_3 \end{vmatrix}$$

$$\bar{q}_3 = \begin{vmatrix} b_1 & k_1 \\ b_3 & k_3 \end{vmatrix} + \begin{vmatrix} c_1 & j_1 \\ c_3 & j_3 \end{vmatrix}$$

$$\bar{q}_4 = \begin{vmatrix} c_1 & k_1 \\ c_3 & k_3 \end{vmatrix}$$

The phase difference and the amplitude ratio between the torsional and flexural motions can be obtained as follows. (See reference 2).

If in the moment equations A1.1 we put $\phi = \bar{\phi}\, e^{i(\omega t+\gamma)}$ and $\theta = \bar{\theta}\, e^{i\omega t}$

then it can be shown that the amplitude ratio is given by

$$\left(\frac{c\,\bar{\theta}}{\ell\,\bar{\phi}}\right)^2 = \frac{b_1c_3 - b_3c_1 - \tilde{\omega}^2(b_1a_3 - b_3a_1)}{j_1k_3 - j_3k_1 - \tilde{\omega}^2(j_1g_3 - j_3g_1)} \qquad \text{.....A1.22}$$

and the phase difference γ from

$$\tan\gamma = \frac{\tilde{\omega}\,(b_3j_1 - b_1j_3)}{(k_1b_3 - k_3b_1) - \tilde{\omega}^2(b_3g_1 - b_1g_3)} \qquad \text{.....A1.23}$$

Since

$$c_1 = \lambda_\phi \int_o^1 f^2\,d\eta + \frac{\ell_\phi}{\rho V^2 \ell^3}$$

$$k_3 = \mu_\theta \int_o^1 F^2\,d\eta + \frac{m_\theta}{\rho V^2 \ell c^2}$$

/we can ...

we can eliminate V^2 and derive that

$$k_3 = \alpha + \beta c_1 \qquad \text{.....A1.24}$$

where

$$\alpha = \mu_\theta \int_o^1 F^2 d\eta - \beta \lambda_\phi \int_o^1 f^2 d\eta$$

$$\beta = \frac{\ell^2 m_\theta}{c^2 \ell_\phi}$$

If k_3 is eliminated from equations A1.20 and A1.21 with the aid of equation A1.24, we obtain the following quadratic equation in terms of the unknown c_1 ,[+] viz.

$$R_1 c_1^2 + R_2 c_1 + R_3 = 0 \qquad \text{.....A1.25}$$

where

$$R_1 = r_1 r_2 - \beta \bar{q}_1^2$$

$$R_2 = r_1 r_3 + r_2 r_4 - \alpha \bar{q}_1^2$$

$$R_3 = r_3 r_4 + k_1 c_3 \bar{q}_1^2$$

and

$$r_1 = b_1 \beta + j_3$$

$$r_2 = (\bar{q}_1 g_3 - \bar{q}_o j_3) + \beta(\bar{q}_1 a_1 - \bar{q}_o b_1)$$

$$r_3 = \bar{q}_1 (b_1 j_3 - b_3 j_1 - a_3 k_1 - c_3 g_1) + \bar{q}_o (b_3 k_1 + c_3 j_1) + \alpha(\bar{q}_1 a_1 - \bar{q}_o b_1)$$

$$r_4 = b_1 \alpha - b_3 k_1 - c_3 j_1$$

If the solution to equation A1.25 is written

$$c_{1c} = - \frac{R_2 \pm \sqrt{R_2^2 - 4R_1 R_3}}{2R_1} \qquad \text{.....A1.26}$$

then the corresponding value for the critical flutter speed V_c is

$$V_c^2 = \frac{\ell_\phi / \rho \ell^3}{c_{1c} - \lambda_\phi \int_o^1 f^2 d\eta} \qquad \text{.....A1.27}$$

/and ...

[+] c_1 and k_3 are unknown since V is initially unknown.

and the non-dimensional frequency parameter

$$\tilde{\omega}_c = \sqrt{\frac{c_{1c}\bar{r}_1 + r_4}{\bar{q}_1}} \qquad \text{.....A1.28}$$

It is interesting to note that the calculation of the flutter speed of a given aerofoil at a number of gap-chord ratios can be obtained approximately by the following method.

It can be shown that for typical values of the aerodynamic derivatives (see figure 21)

$$c_1 = A\,\alpha + B\,k_1 \qquad \text{.....A1.29}$$

where the constants A and B (not to be confused with A and B used in equation 2.35) can be obtained from an evaluation of c_1 from equation A1.26 for say the aerofoil in the isolated case when arbitrary values are in turn inserted for α and k_1.

Hence

$$c_1 - \lambda_\phi \int_0^1 f^2 d\eta = Bk_1 + A\mu_\theta \int_0^1 f^2 d\eta - (A\beta+1)\lambda_\phi \int_0^1 f^2 d\eta$$

.....A1.30

and from equation A1.27

$$V_c^2 = \frac{I_\alpha / \rho l^3}{Bk_1 + A\mu_\theta \int_0^1 F^2 d\eta - A\beta\lambda_\phi \int_0^1 f^2 d\eta} \qquad \text{.....A1.31}$$

Similarly

$$\tilde{\omega}^2 = C\,\alpha + Dk_1 \qquad \text{.....A1.32}$$

where C and D are constants.

Therefore, having calculated A, B, C and D, and knowing the values of λ_θ, μ_θ, λ_ϕ for various gap-chord ratios, the corresponding values of V_c and $\tilde{\omega}$ can be directly obtained from the equations above.

The critical flutter speed and frequency have been estimated, by the method described above, for the aerofoils used in these tests. Typical results are given in table II below.

/Table II ...

TABLE II

Aerofoil properties	Theoretical	Experimental	
	Assumed values	Aerofoil 11	Aerofoil 14
chord c	3.0 in.	3.0 in.	3.0 in.
span ℓ	8.0 in.	8.0 in.	8.0 in.
t/c	0.10	0.10	0.10
Flexural stiffness l_ϕ	3.01b.ft/rad.	2.491b.ft/rad.	2.721b.ft/rad.
ω_f	205 rad/sec.	152 rad/sec.	179.5 rad/sec.
Torsional stiffness m_θ	0.161b.ft/rad.	0.151b.ft/rad.	0.1751b.ft/rad.
ω_t	484 rad/sec.	326 rad/sec.	326 rad/sec.
	Calculated		
Critical flutter speed	97.5 f.p.s.	87 f.p.s.	111 f.p.s
Critical flutter frequency	272 rad/sec.	220 rad/sec.	277 rad/sec.
Frequency parameter	0.7	1.0	1.0

APPENDIX 2

An approximate calculation of the forces arising from the finite amplitude of oscillating aerofoils in cascade

§A.1. Introduction

In the classical treatment of the forces arising on an isolated oscillating aerofoil, the assumption is made that the amplitude of the oscillations is infinitesimal. The results so obtained are, however, applicable to aerofoils oscillating with finite amplitude, provided that the amplitude is small compared with, say, the aerofoil chord.

When the classical theory is extended to the case of oscillating aerofoils in cascade, where adjacent aerofoils have antiphase motions, the results, so obtained, are not directly applicable to the case of small, but finite, amplitude. In fact, the classical theory neglects the small, but important change in the tangential velocity components in the neighbourhood of the aerofoils due to the changing gap between adjacent oscillating aerofoils. This effect will naturally be important only for cascades of oscillating aerofoils having small gap-chord ratio.

/A very ...

A very crude approximation is given below of the forces and moments on an oscillating aerofoil in cascade due to these changes in the tangential velocity above and below the aerofoil. It will be assumed that such forces and moments will be additive to those calculated on the basis of the classical theory.

It is not suggested that the numerical values calculated from this crude theory are necessarily good approximations to the exact results. It is hoped, however, that they will give the order of the corrections involved, and will serve to stimulate further interest in this problem.+

§A.2. Analysis

Let us consider a two-dimensional cascade of aerofoils, having zero thickness, which are set at zero incidence and stagger angle. We will assume that adjacent aerofoils are vibrating with antiphase motions.*

Let the amplitude of the displacement of the aerofoil, with reference axis at the mid chord positions, and the instantaneous displacement be respectively

$$\bar{z} = \bar{z}_0 + x\,\bar{\theta} \qquad \text{.....A2.1}$$

and

$$z = \bar{z}\, e^{i\omega t} \qquad \text{.....A2.2}$$

Let us consider aerofoil (0), see figure 22, which at time t has a displacement z at distance x from the origin. At this latter station let the velocities above and below aerofoil (0) be uniform and equal to $V-u$ and $V+u$ respectively. After the time interval dt the fluid which crossed the plane at x, at time t, will have moved to $x + dx$,‡ where the velocities above and below the aerofoil will be equal to $V-u-du$ and $V+u+du$ respectively. The corresponding change in the aerofoil

/displacement

+ The problem of the forces and moments arising on two adjacent oscillating spheres has been discussed by Lamb (reference 8).

* The axes and notation are similar to that used in Part 2.

‡ The small difference between the relative movements of the fluid above and below the aerofoil has been neglected in this crude approximation.

displacement will be dz. Since the rates of mass flow at times t and t+dt must be equal

$$(V+u)\left(\frac{s}{2} - z\right) = (V+u+du)\left(\frac{s}{2} - z - dz\right)$$

below the aerofoil and A2.3

$$(V-u)\left(\frac{s}{2} + z\right) = (V-u-du)\left(\frac{s}{2} + z + dz\right)$$

above the aerofoil.

When $|z| << s/2$ the required solution of equations A2.3 is

$$\frac{u}{V} = \frac{2z}{s} \qquad \text{.....A2.4}$$

giving

$$u_+ - u_- = -\frac{4Vz}{s} \qquad \text{.....A2.5}$$

where u_+ and u_- are respectively the perturbation velocities above and below the aerofoil.

From Bernoulli's equation for the unsteady flow of an incompressible fluid, when second order velocity components are neglected, it can be shown that,+

$$p_+ - p_- = \frac{4\rho V^2}{s}\left(\zeta + x\theta\right) + i\omega\frac{4\rho V}{s}\left[\left(x + \frac{c}{2}\right)\zeta + \left(x^2 - \frac{c^2}{4}\right)\frac{\theta}{2}\right]$$

.....A2.6

The amplitude of the lift force is given by

$$-\frac{\bar{Z}}{\pi\rho c V^2} = -\frac{4\bar{\zeta}/c}{\pi s/c} - \frac{i\tilde{\omega}}{\pi s/c}\left(2\bar{\zeta}/c - \bar{\theta}/3\right) \qquad \text{.....A2.7}$$

and the amplitude of the pitching moment about the mid-chord axis is

$$-\frac{\bar{M}}{\pi\rho c^2 V^2} = -\frac{\bar{\theta}}{3\pi s/c} - \frac{i\tilde{\omega}}{3\pi s/c}\,\bar{\zeta}/c \qquad \text{.....A2.8}$$

The airload coefficients are

$$\bar{Z}_{12} = -\frac{4}{\pi s/c} - \frac{2i\tilde{\omega}}{\pi s/c} \;;\quad \bar{Z}_{34} = \frac{i\tilde{\omega}}{3\pi s/c}$$

$$\bar{M}_{12} = -\frac{i\tilde{\omega}}{3\pi s/c} \;;\quad \bar{M}_{34} = -\frac{1}{3\pi s/c} \qquad \text{.....A2.9}$$

/and the ...

+ The pressure difference calculated from equations A2.6 must be added, as stated in the introductory remarks, to the pressure difference caused by the direction motion of the aerofoil.

and the lift and pitching moment derivatives about the mid-chord axis are,

$$\ell_z = -\frac{4}{s/c} \quad ; \quad \ell_{\dot{z}} = -\frac{2}{s/c}$$

$$\ell_\theta = 0 \quad ; \quad \ell_{\dot{\theta}} = \frac{1}{3s/c}$$

$$m_z = 0 \quad ; \quad m_{\dot{z}} = -\frac{1}{3s/c} \qquad \text{.....A2.10}$$

$$m_\theta = -\frac{1}{3s/c} \quad ; \quad m_{\dot{\theta}} = 0$$

If we now compare the derivatives above with those obtained by the classical theory (see equation 2.51) it can be seen that both the classical stiffness and damping derivatives are reduced when the reference axis is forward of the mid-chord.

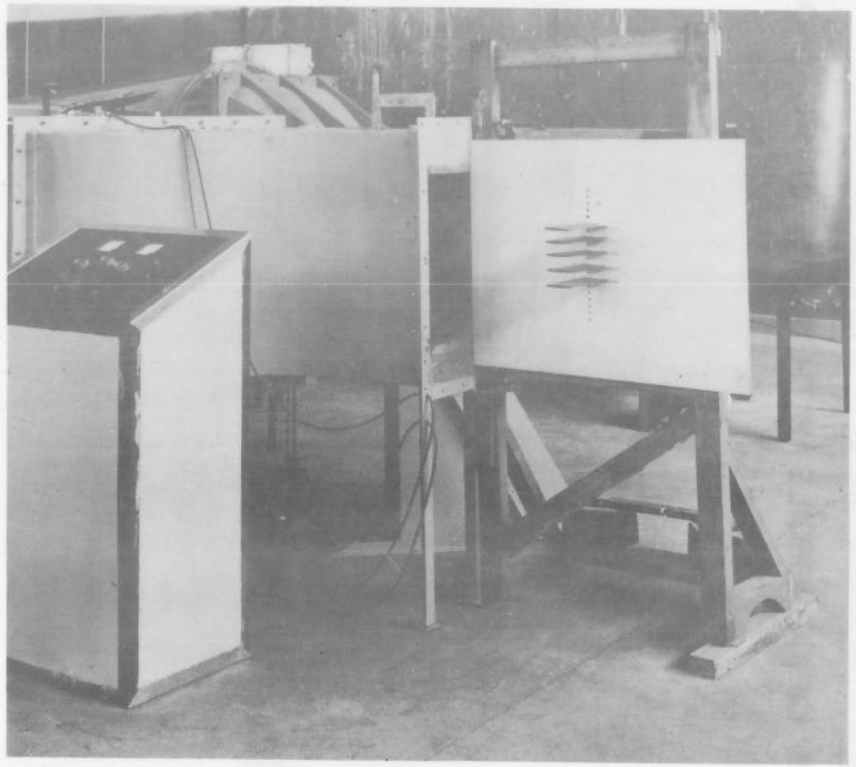

VIEW OF THE TUNNEL SHOWING THE UNSTAGGERED CASCADE IN POSITION.

FIG. 1.

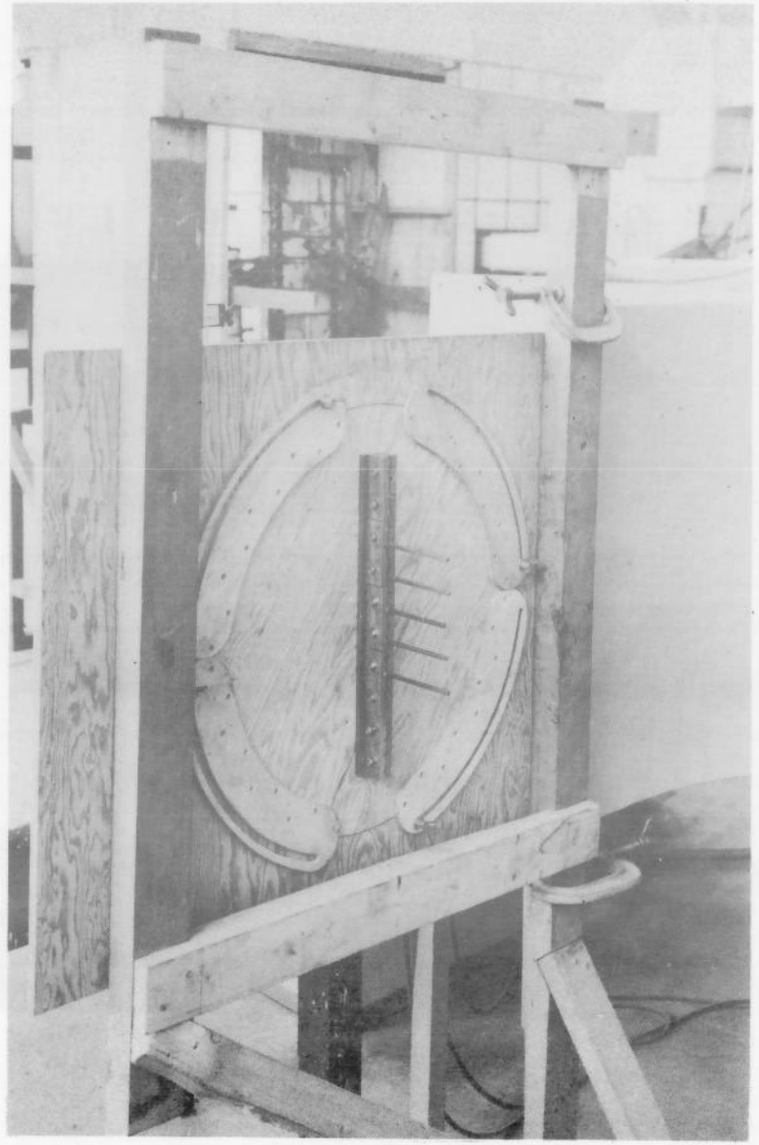

BACK OF THE TURNTABLE SHOWING BLOCKS FOR CLAMPING THE AEROFOILS.

FIG. 2.

FIGS. 3 & 4.

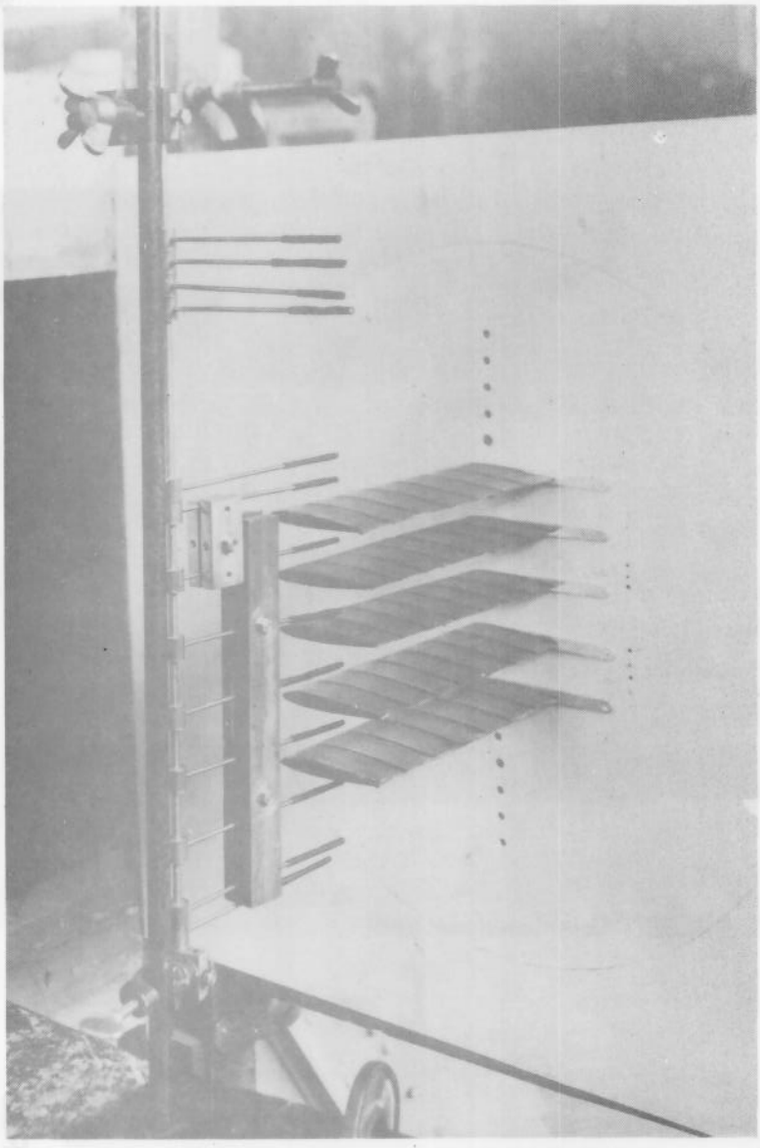

CASCADE OF AEROFOILS WITH STOPS IN POSITION
FIG. 3.

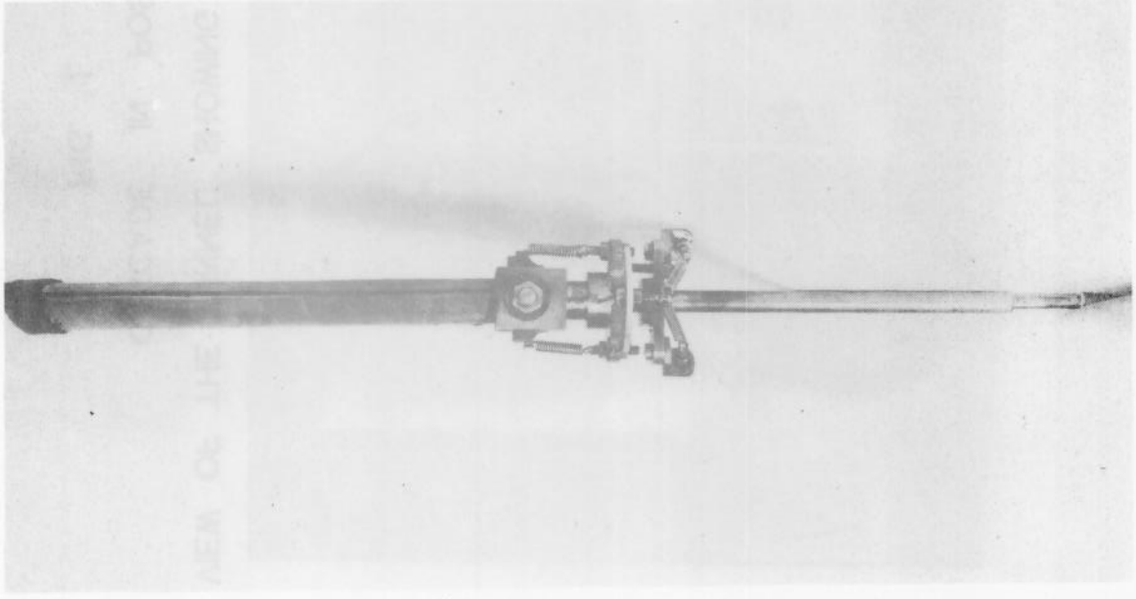

GENERAL VIEW OF THE METAL BLADE SHOWING THE FLEXURE-TORSION SPRINGS AT THE ROOT FIXING
FIG. 4.

FIG. 5.

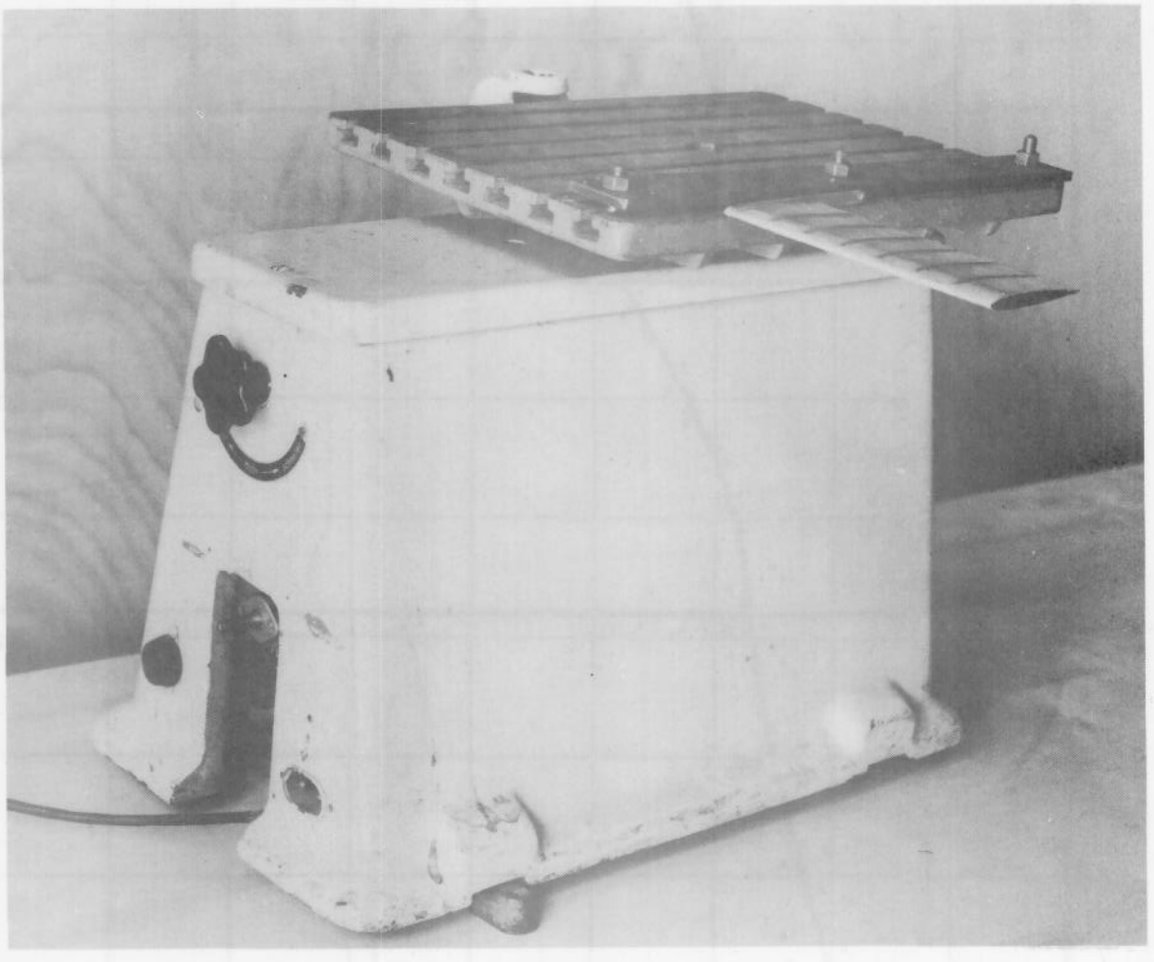

VIEW OF THE AEROFOIL MOUNTED ON THE VIBRATION TABLE.

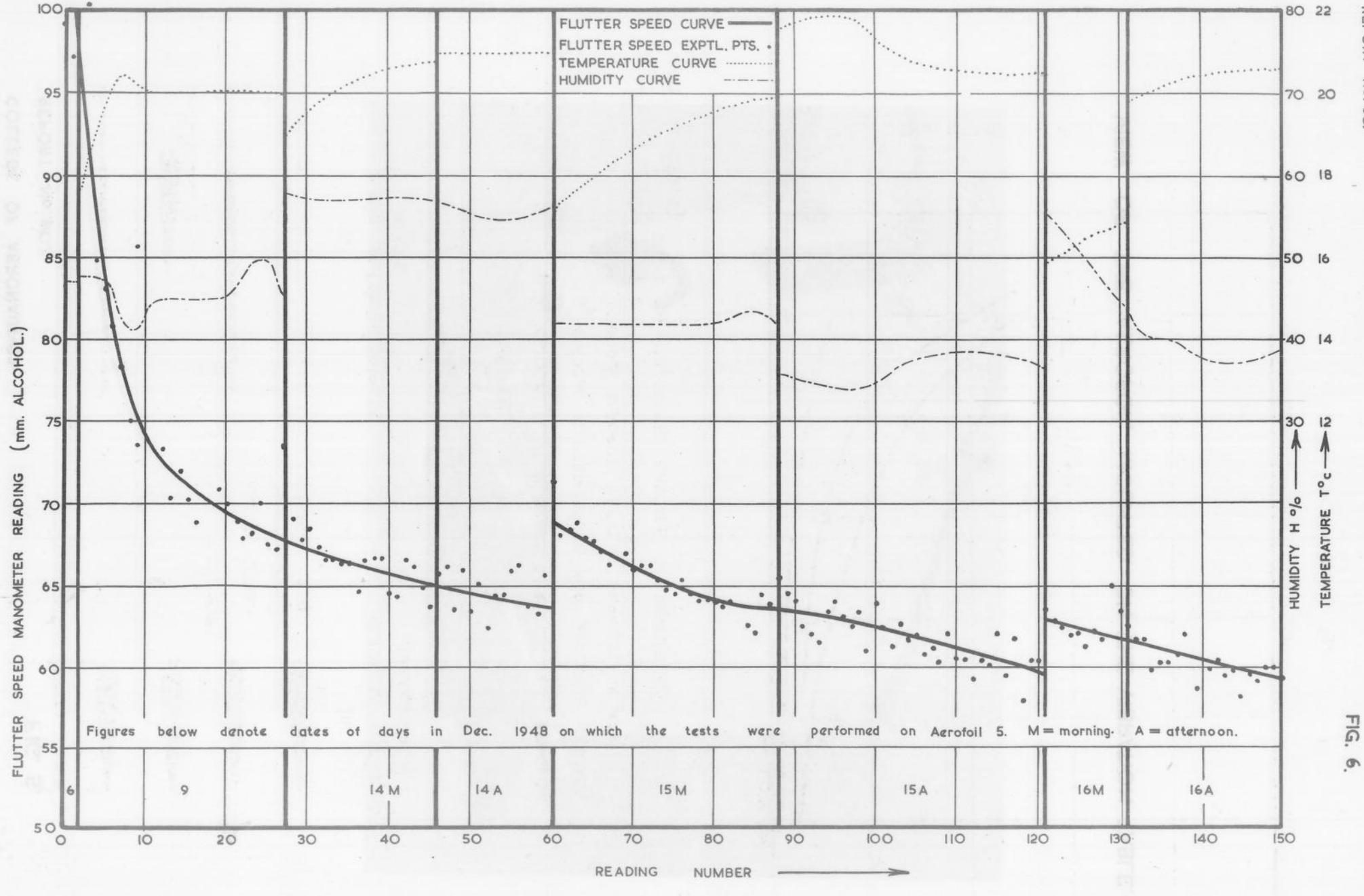

FIG. 6.

DECLINE IN FLUTTER SPEED WITH AGE

COLLEGE OF AERONAUTICS.

REPORT No. 60.

FIG. 7.

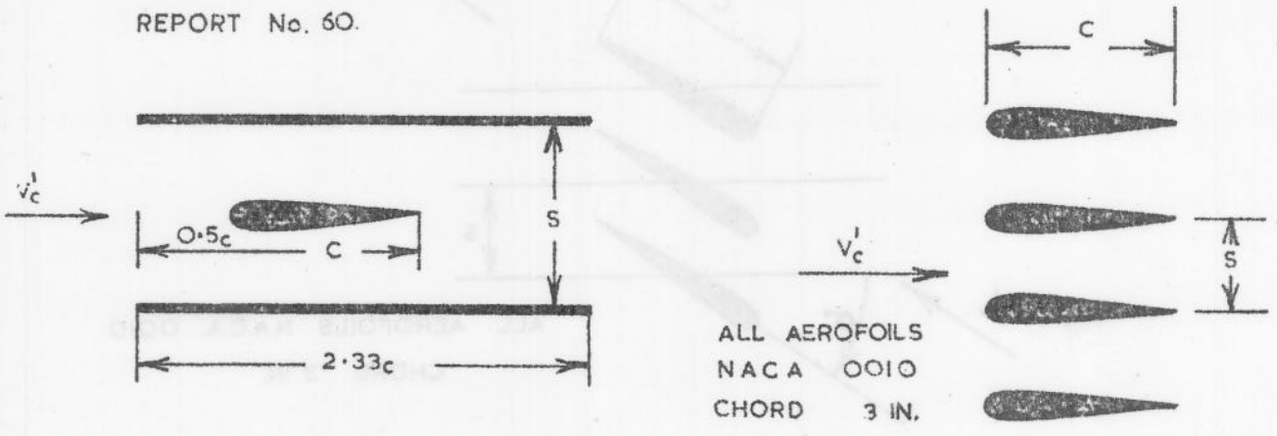

(a)
SINGLE AEROFOIL BETWEEN PARALLEL PLATES.

(b)
AEROFOILS IN CASCADE (UNSTAGGERED)

LEGEND.

V_c CRITICAL FLUTTER SPEED FOR ISOLATED AEROFOIL.

V_c' CRITICAL FLUTTER SPEED FOR AEROFOIL CASCADE.

○ CURVE (a) SINGLE AEROFOIL BETWEEN PARALLEL PLATES.

△ 5 AEROFOILS, □ 6 AEROFOILS } CURVE (b) UNSTAGGERED CASCADE OF AEROFOILS.

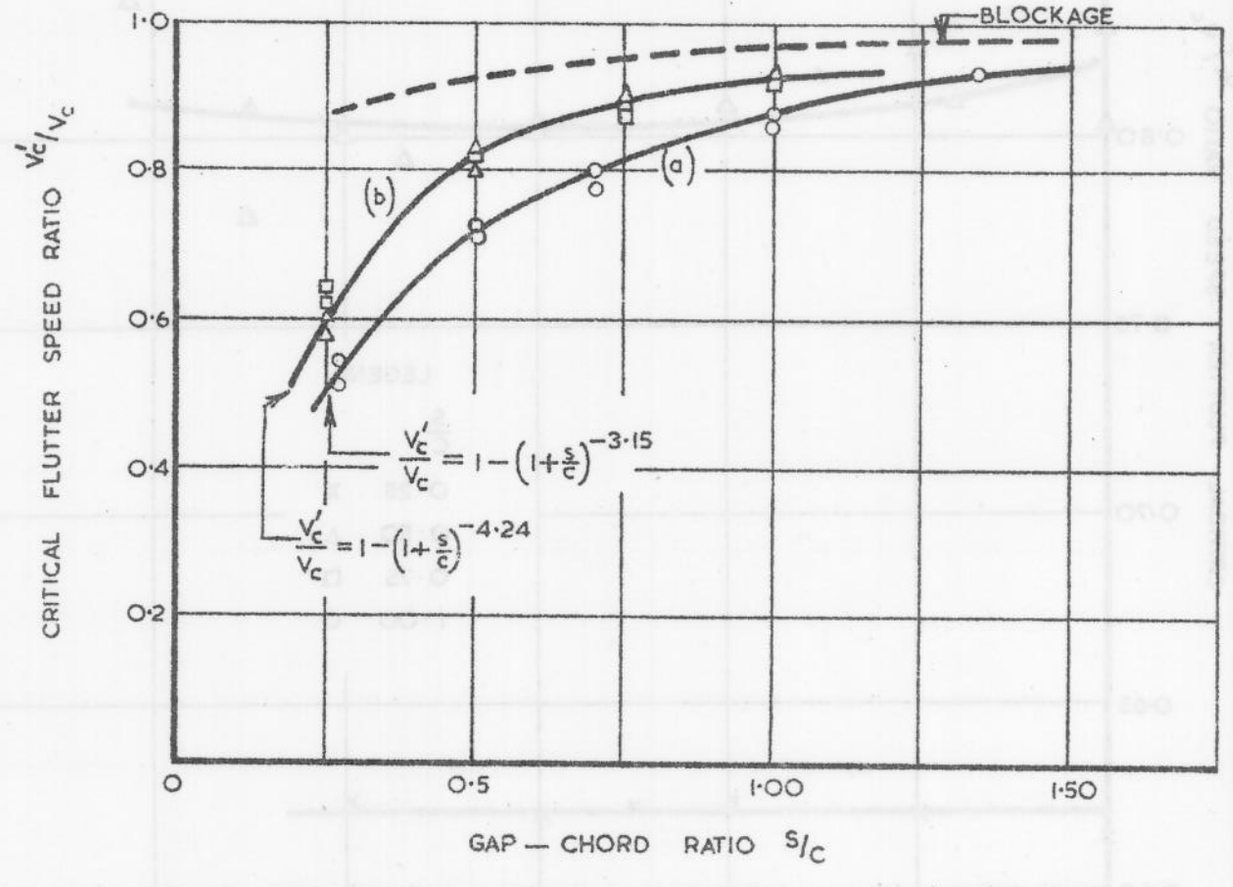

CRITICAL FLUTTER SPEED VARIATION WITH GAP CHORD RATIO.

FIG. 8.

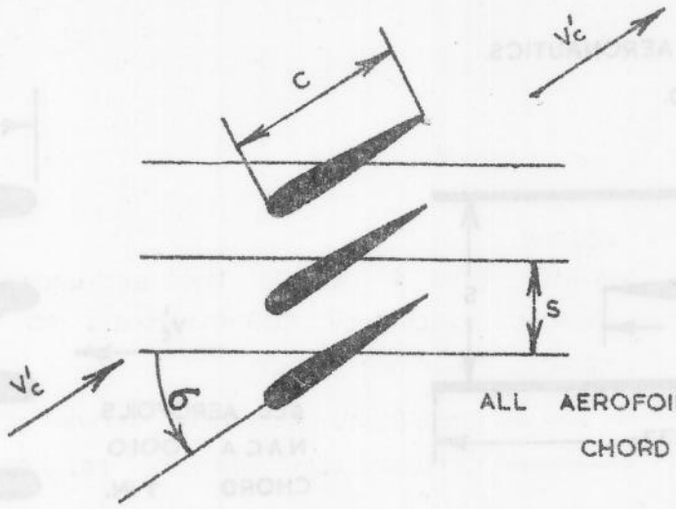

ALL AEROFOILS N.A.C.A. 0010
CHORD 3 IN.

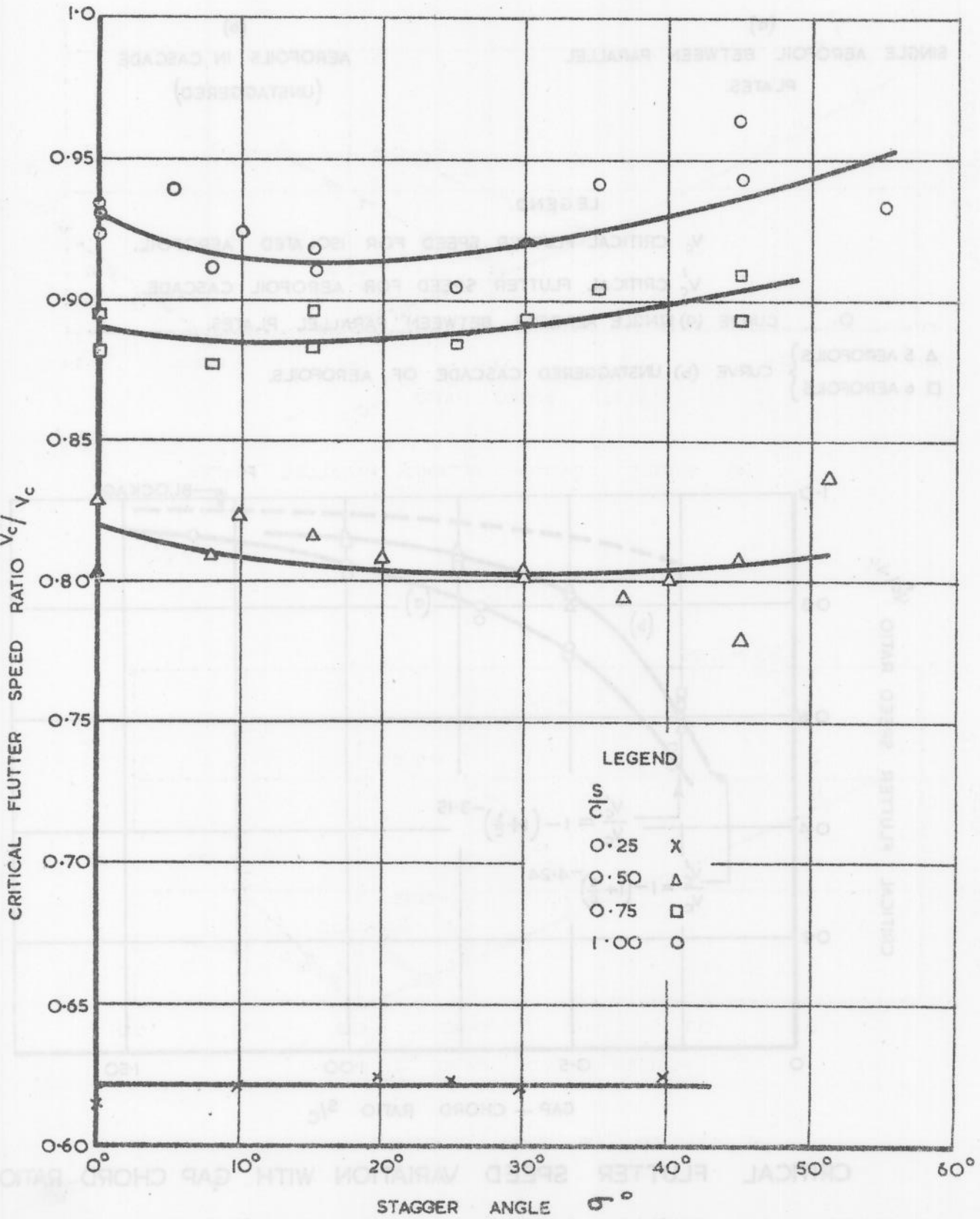

CRITICAL FLUTTER SPEED VARIATION WITH STAGGER ANGLE.

FIG. 9.

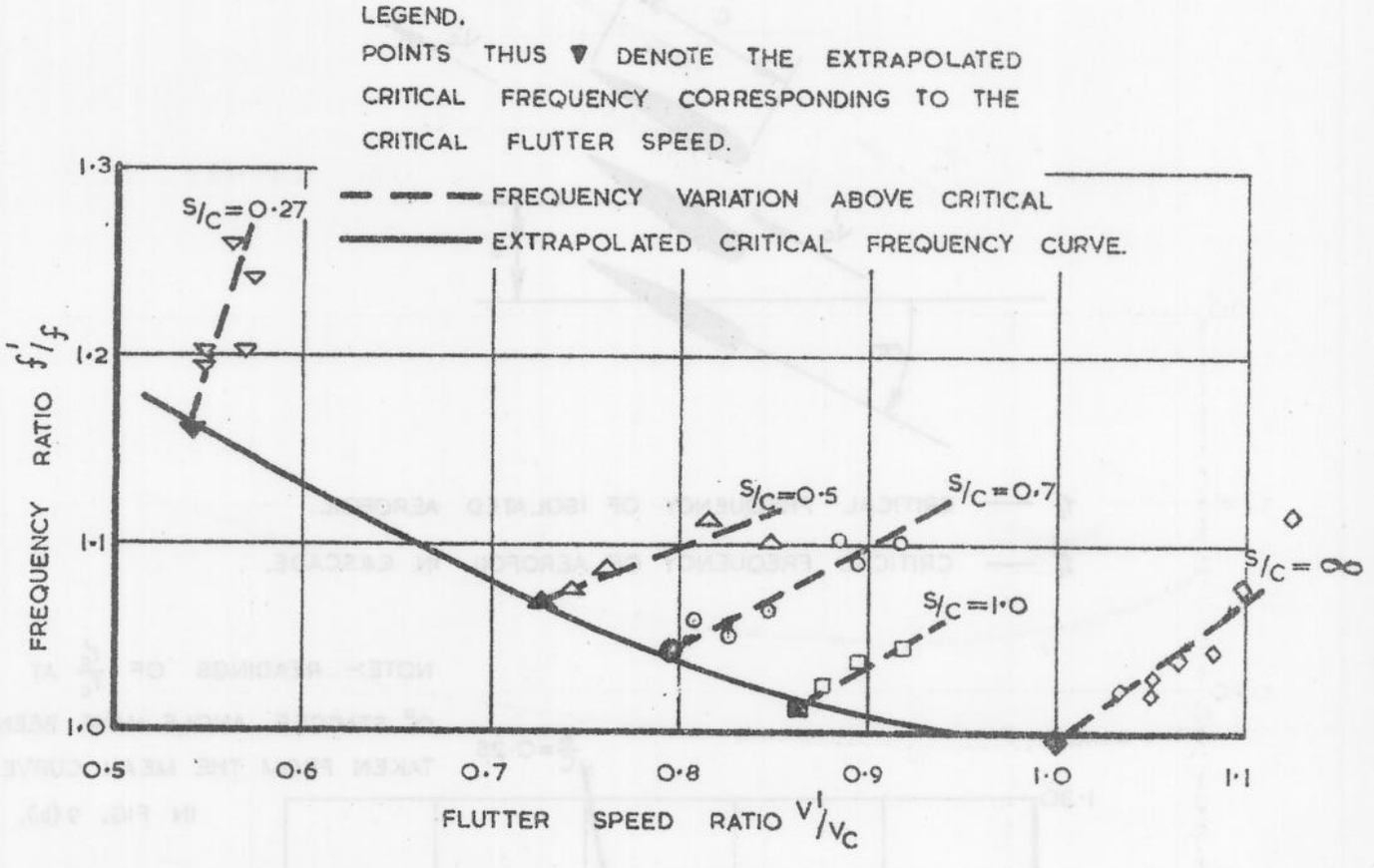

(a) SINGLE AEROFOIL BETWEEN PARALLEL PLATES.

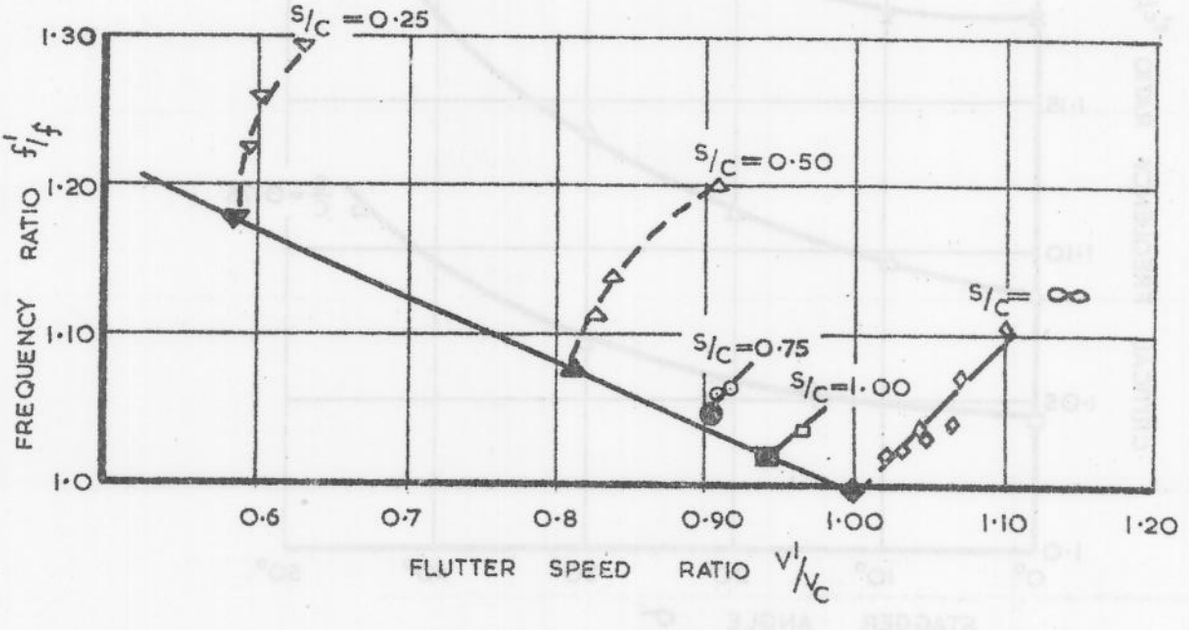

(b). CASCADE OF FIVE AEROFOILS.

VARIATION OF CRITICAL FREQUENCY WITH GAP-CHORD RATIO.

COLLEGE OF AERONAUTICS.
REPORT No. 60.

FIG. 10.

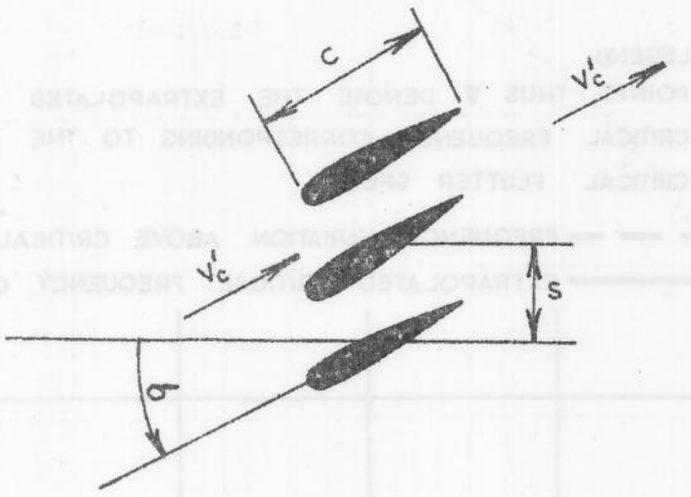

f_c —— CRITICAL FREQUENCY OF ISOLATED AEROFOIL.

f_c' —— CRITICAL FREQUENCY OF AEROFOIL IN CASCADE.

NOTE:- READINGS OF $\frac{f_c'}{f_c}$ AT 0° STAGGER ANGLE HAVE BEEN TAKEN FROM THE MEAN CURVE IN FIG. 9 (b).

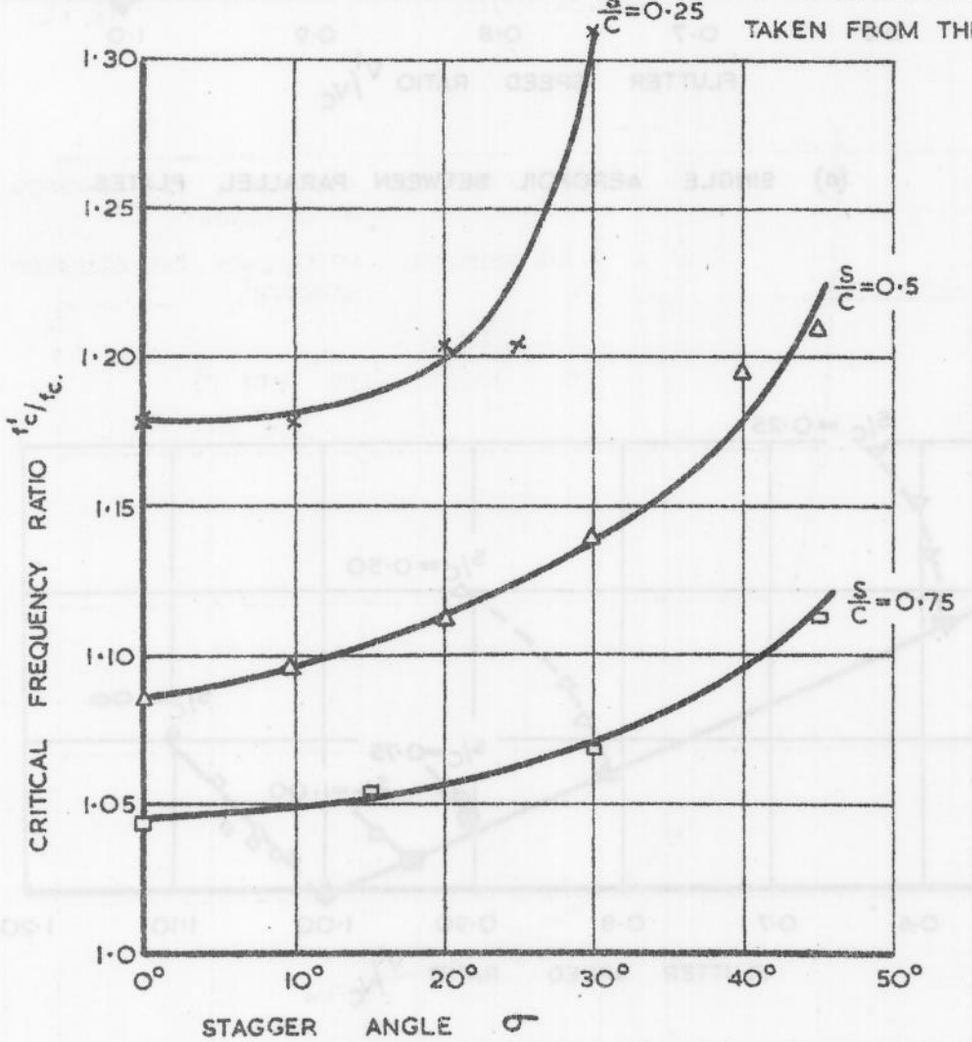

VARIATION OF CRITICAL FREQUENCY WITH GAP–CHORD RATIO AND STAGGER ANGLE.

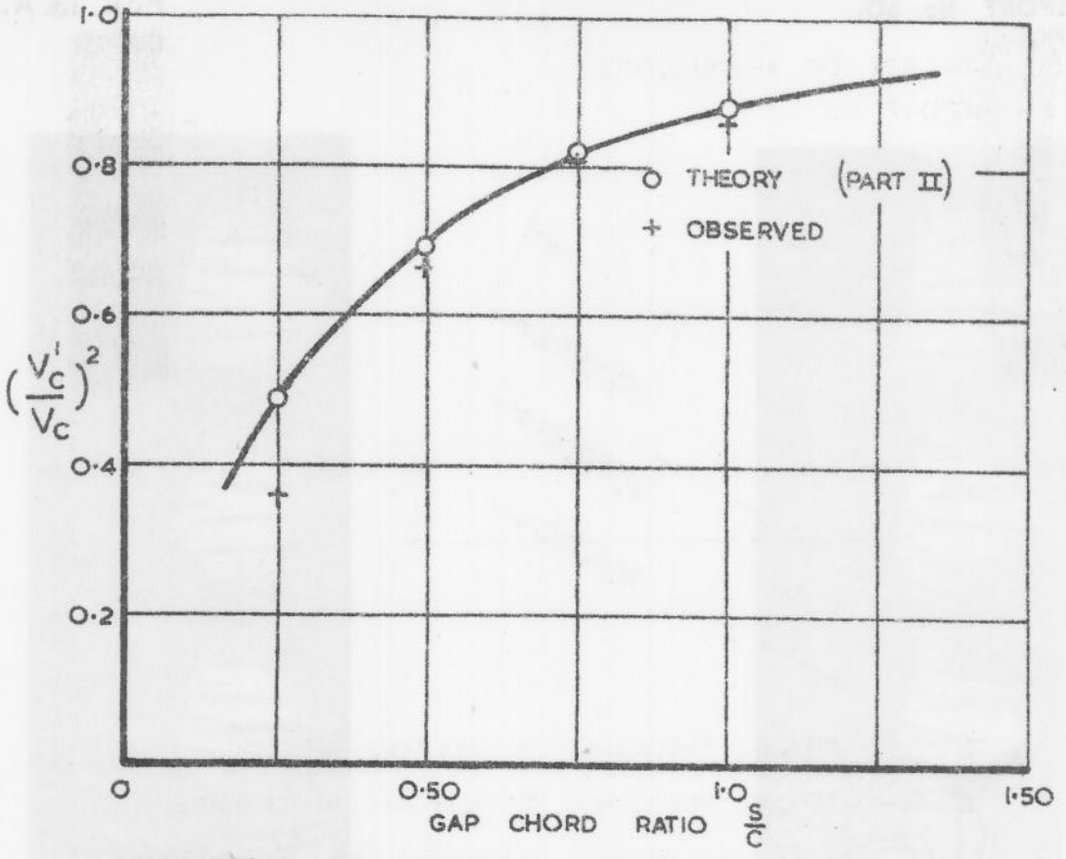

VARIATION OF CRITICAL FLUTTER SPEED WITH GAP–CHORD RATIO FOR THE UNSTAGGERED CASCADE.

FIG. 11.

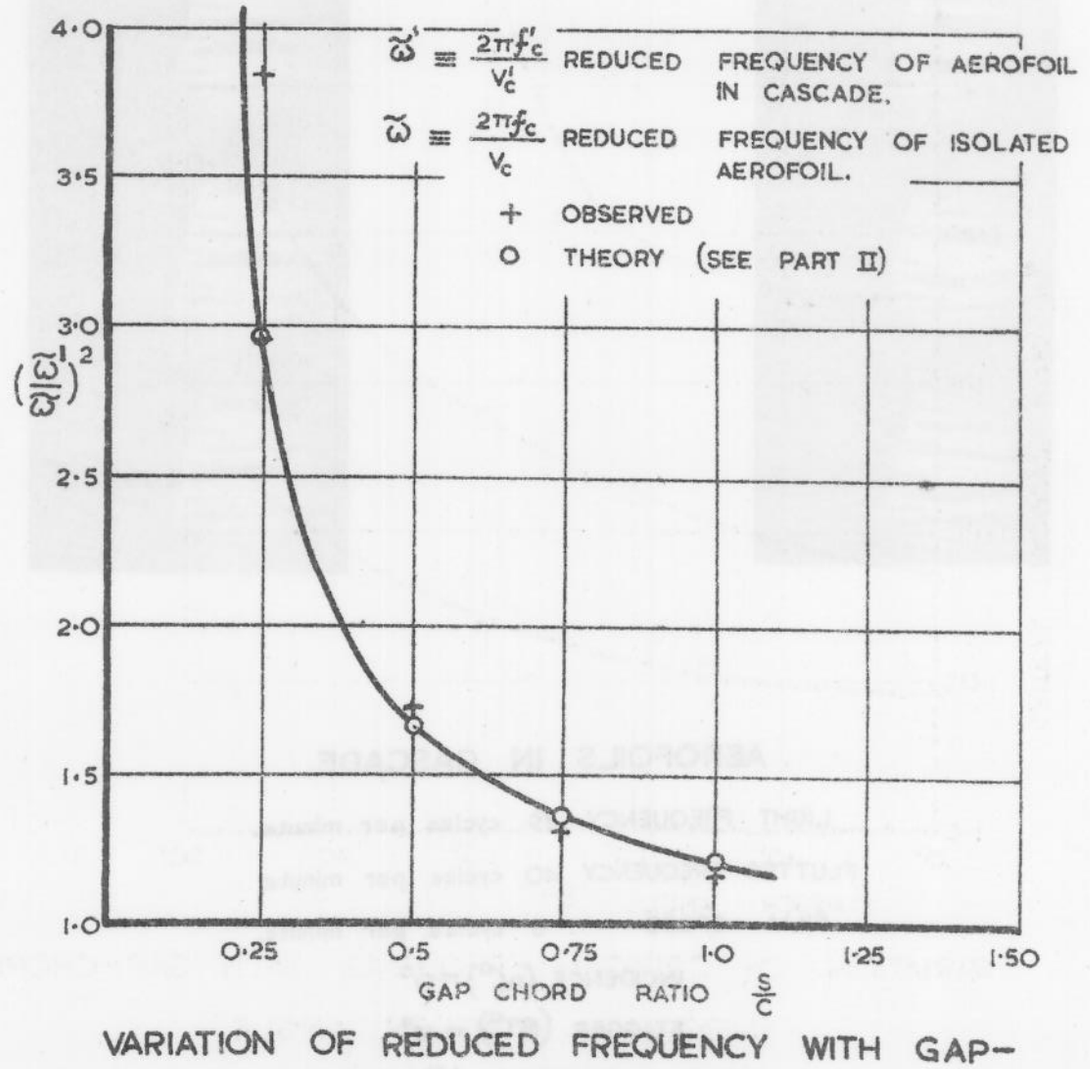

VARIATION OF REDUCED FREQUENCY WITH GAP–CHORD RATIO FOR THE UNSTAGGERED CASCADE.

FIG. 12.

FIG. 13. A.

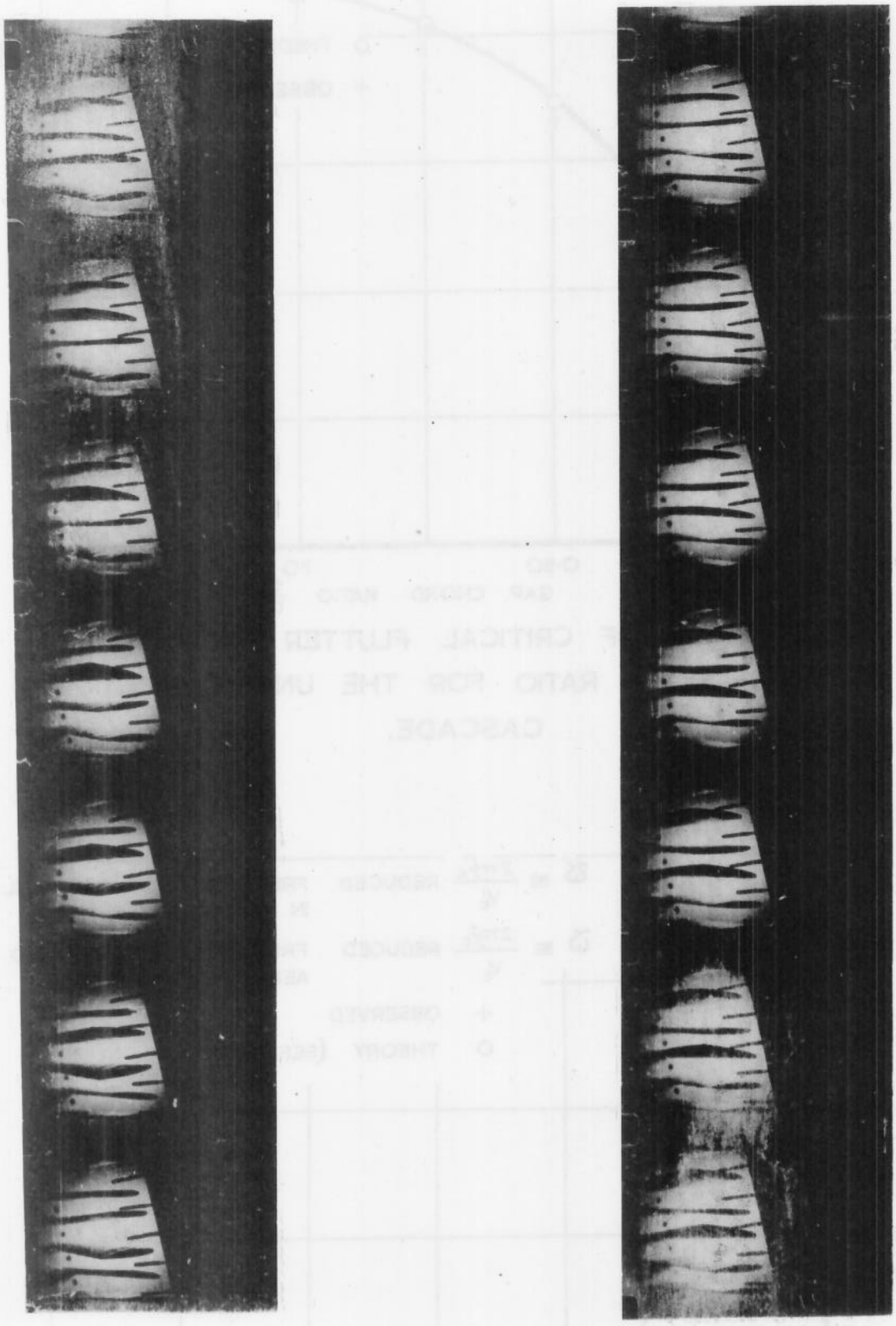

AEROFOILS IN CASCADE.

LIGHT FREQUENCY 39 cycles per minute.

FLUTTER FREQUENCY 40 cycles per minute.

FILM SPEED 8 cycles per minute.

INCIDENCE $(\alpha^\circ) = 0^\circ$

STAGGER $(\sigma^\circ) = 15^\circ$

GAP—CHORD RATIO $\left(\frac{s}{c}\right) = 0.5$

FIG 13. B.

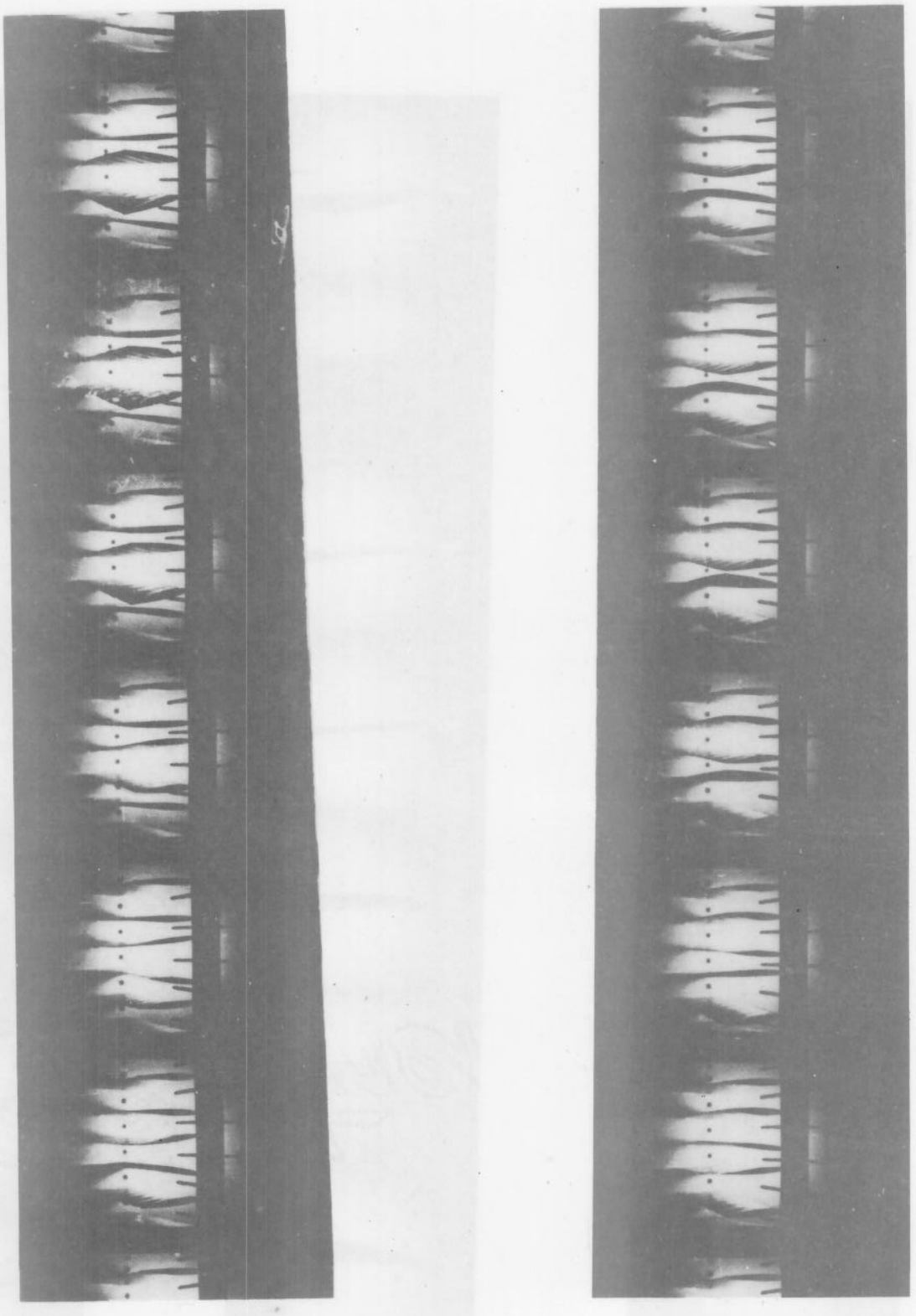

AEROFOILS IN CASCADE.

LIGHT FREQUENCY 39 cycles per minute.

FLUTTER FREQUENCY 40 cycles per minute.

FILM SPEED 8 cycles per minute.

INCIDENCE $(\alpha^\circ) = 0^\circ$

STAGGER $(\sigma^\circ) = 15^\circ$

GAP – CHORD RATIO $(\frac{s}{c}) = 0{\cdot}5$

FIG. 13.C.

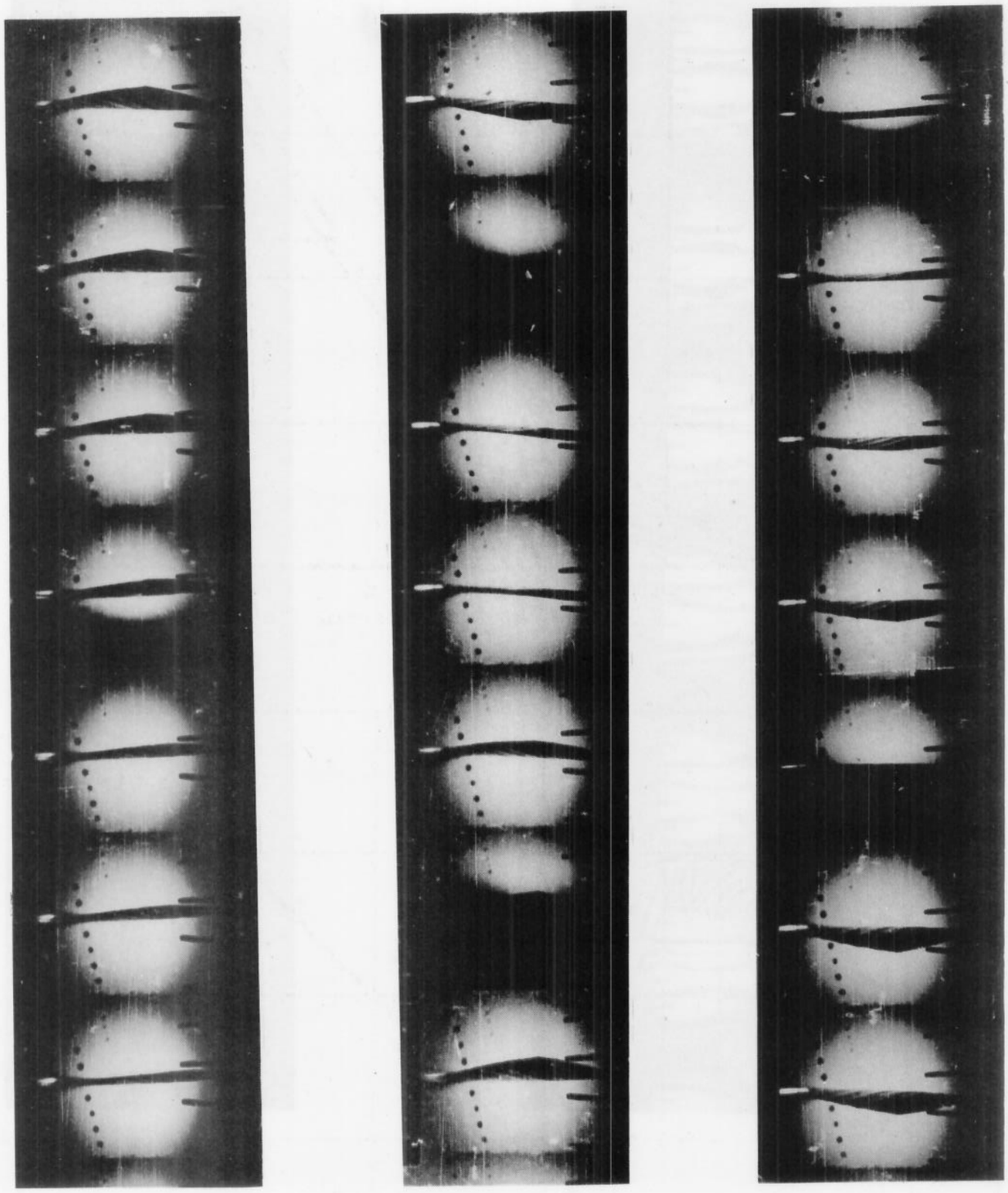

ISOLATED AEROFOIL.

LIGHT FREQUENCY 39 cycles per second.

FLUTTER FREQUENCY 40 cycles per second.

FILM SPEED 8 cycles per second.

INCIDENCE (α°) = 0°

FIG. 14A. & 14B.

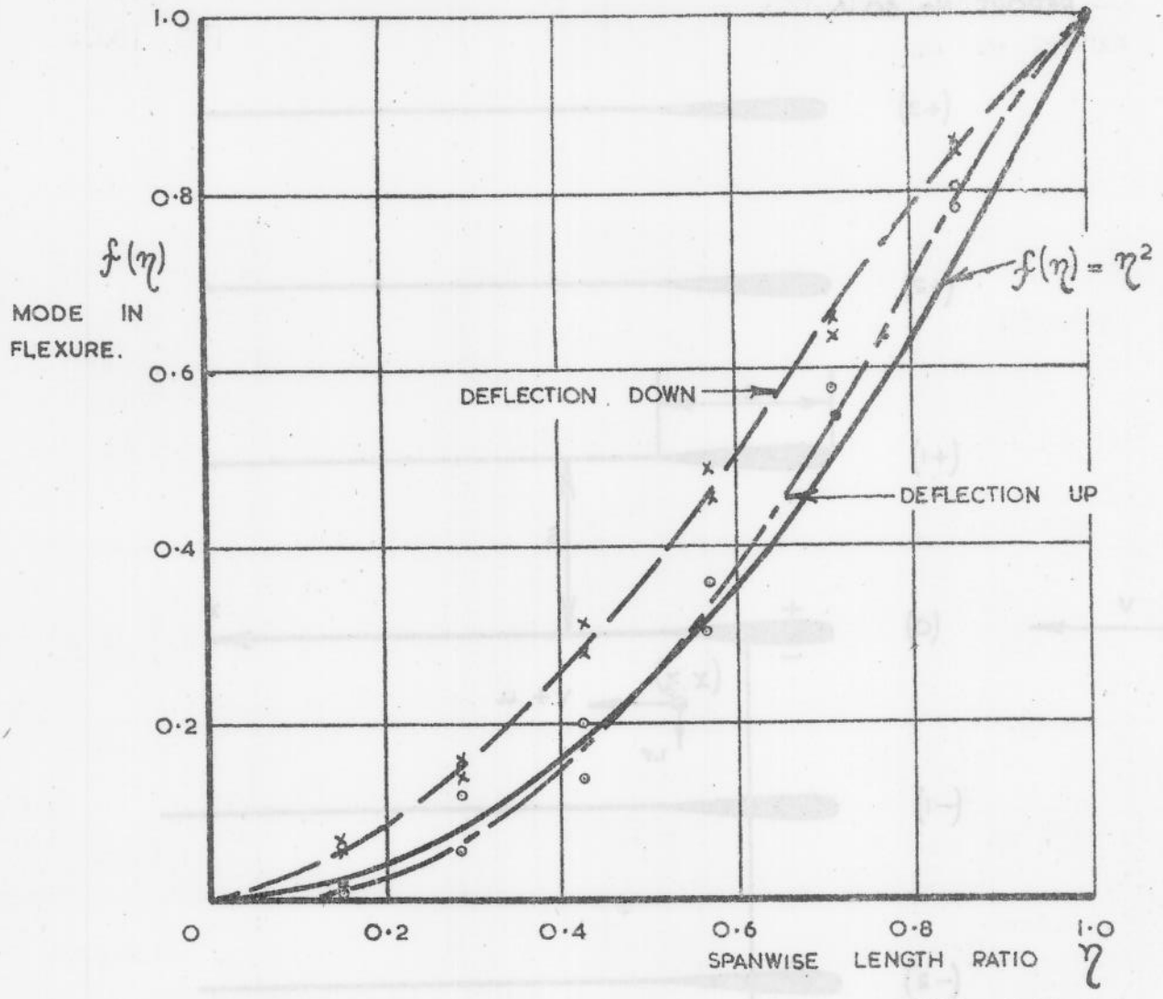

FIG. 14 A.

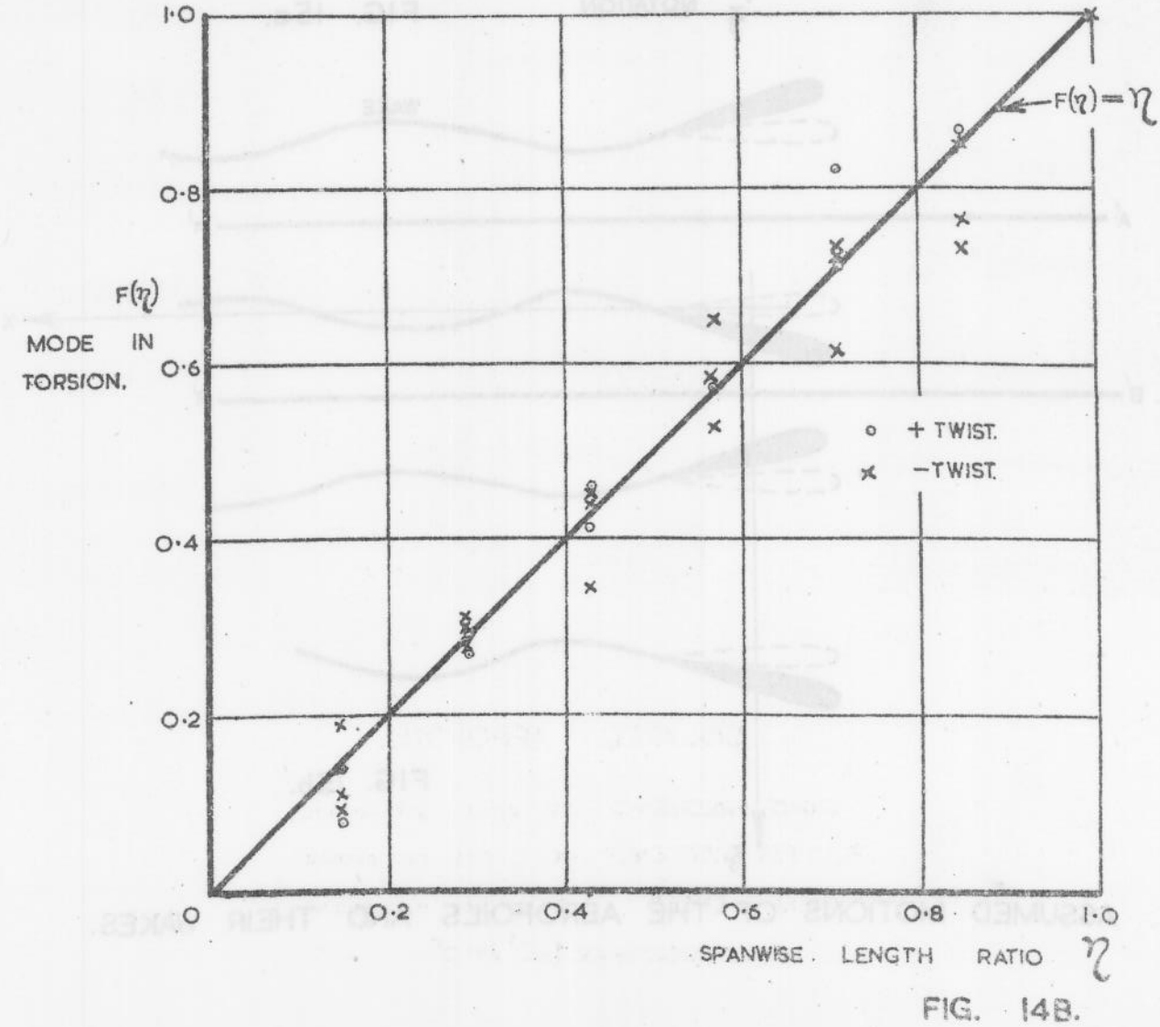

FIG. 14B.

FIGS. 15a. & 15b.

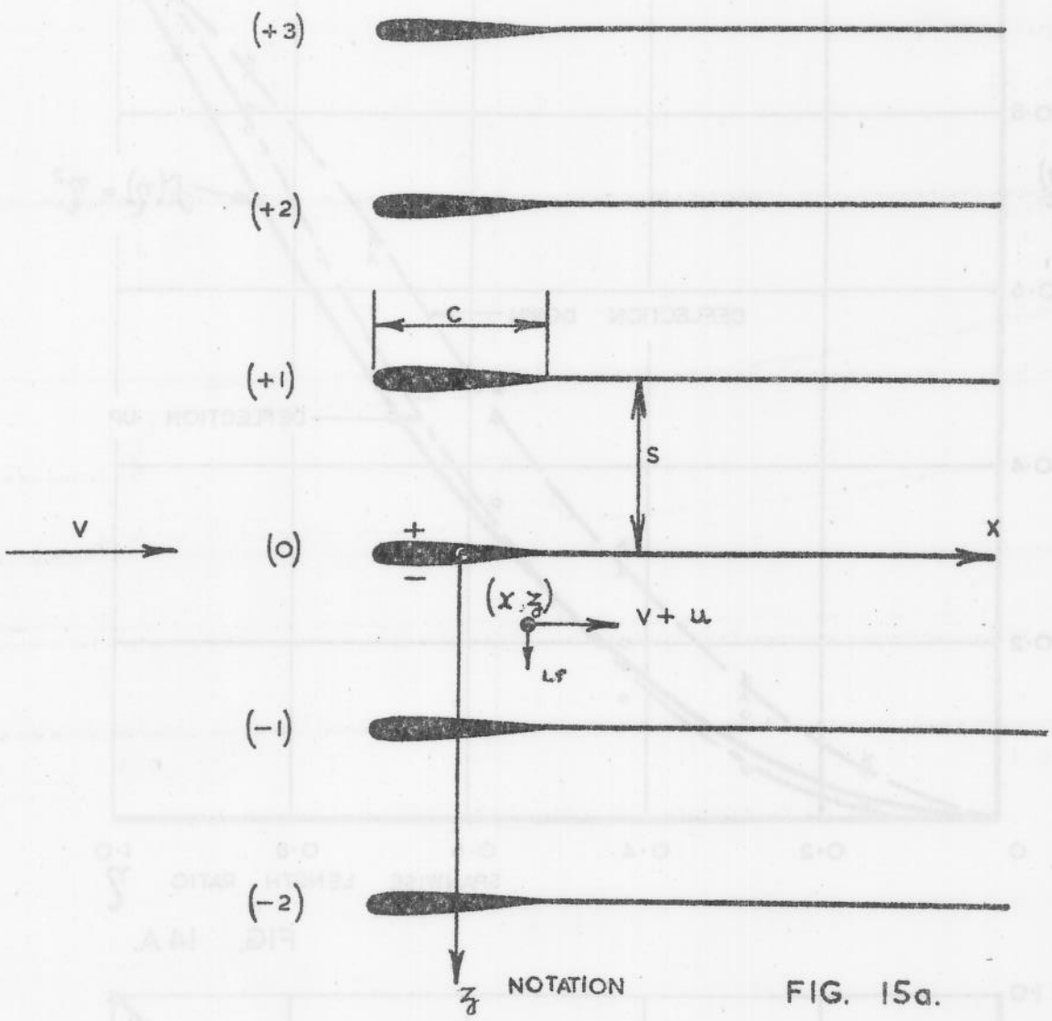

NOTATION

FIG. 15a.

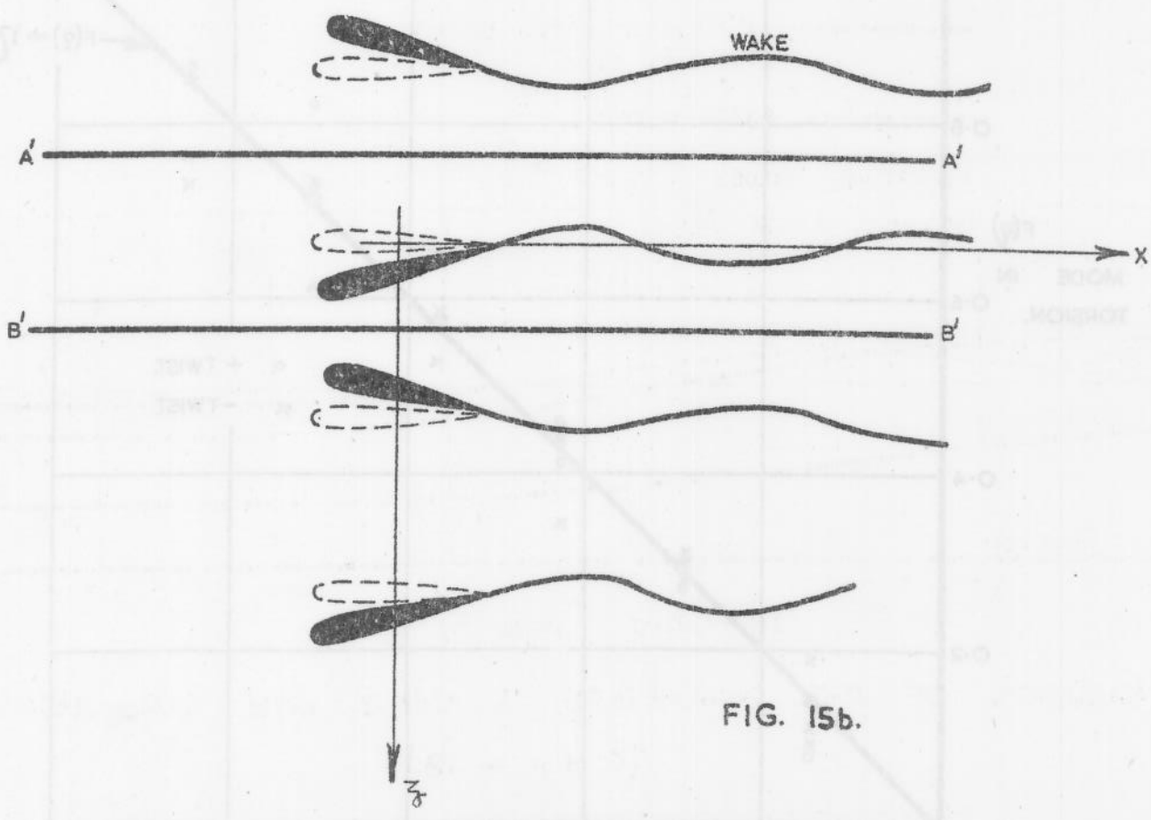

FIG. 15b.

ASSUMED MOTIONS OF THE AEROFOILS AND THEIR WAKES.

COLLEGE OF AERONAUTICS

REPORT No. 60.

FIG. 16.

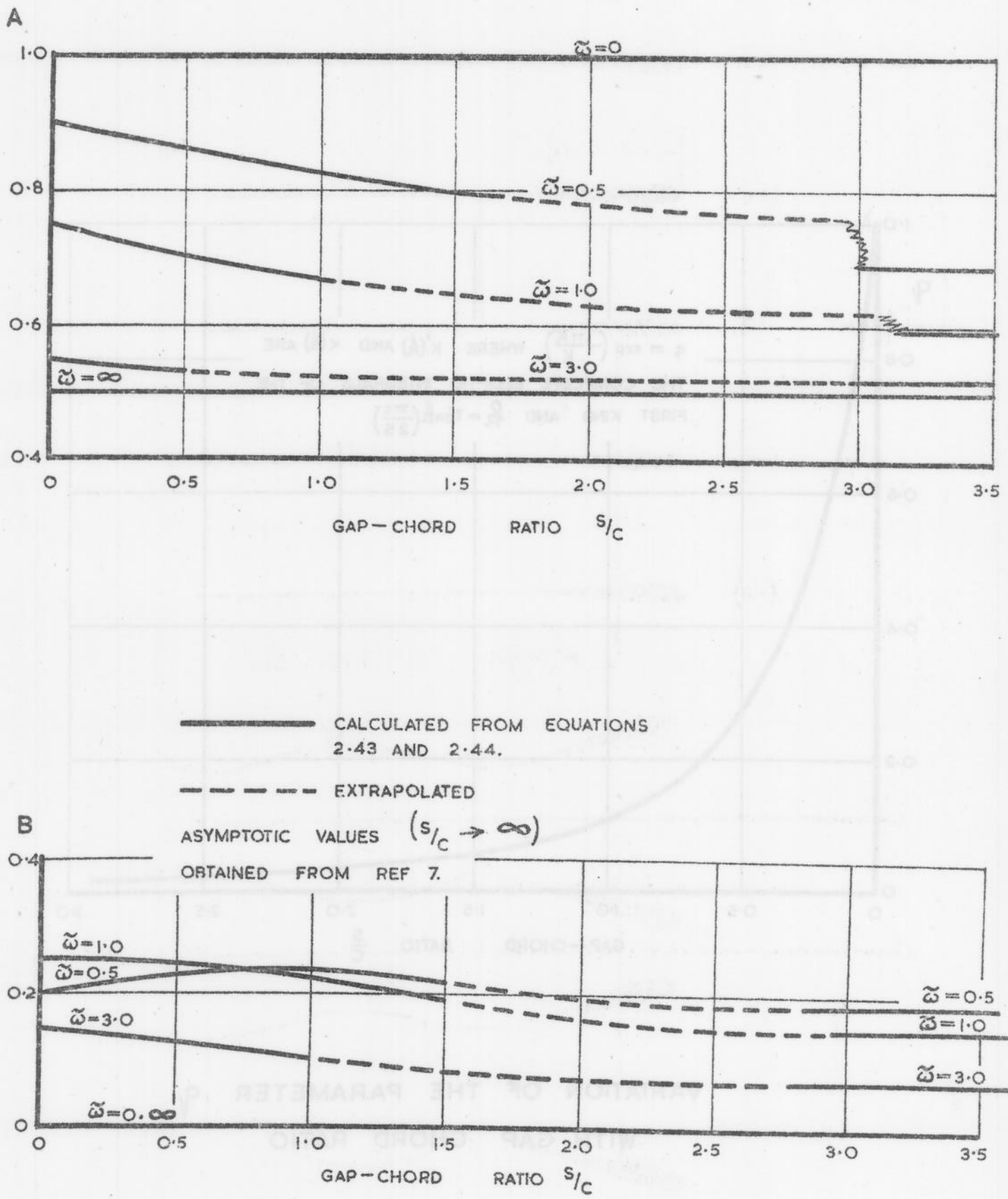

VARIATION OF THE PARAMETERS A AND B WITH GAP—CHORD RATIO.

$(C \equiv A - iB.)$

FIG. 17.

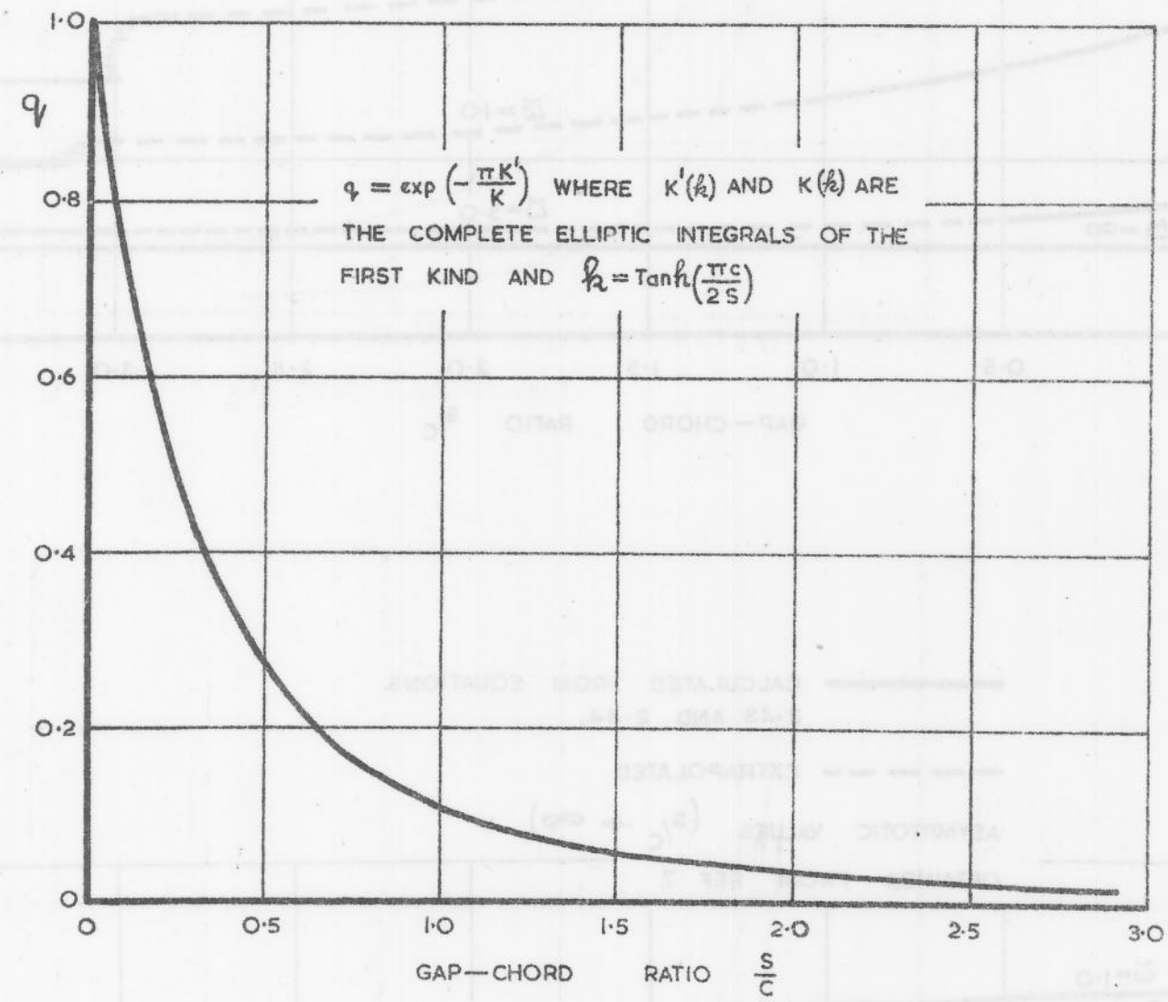

VARIATION OF THE PARAMETER q
WITH GAP CHORD RATIO

FIG. 18.

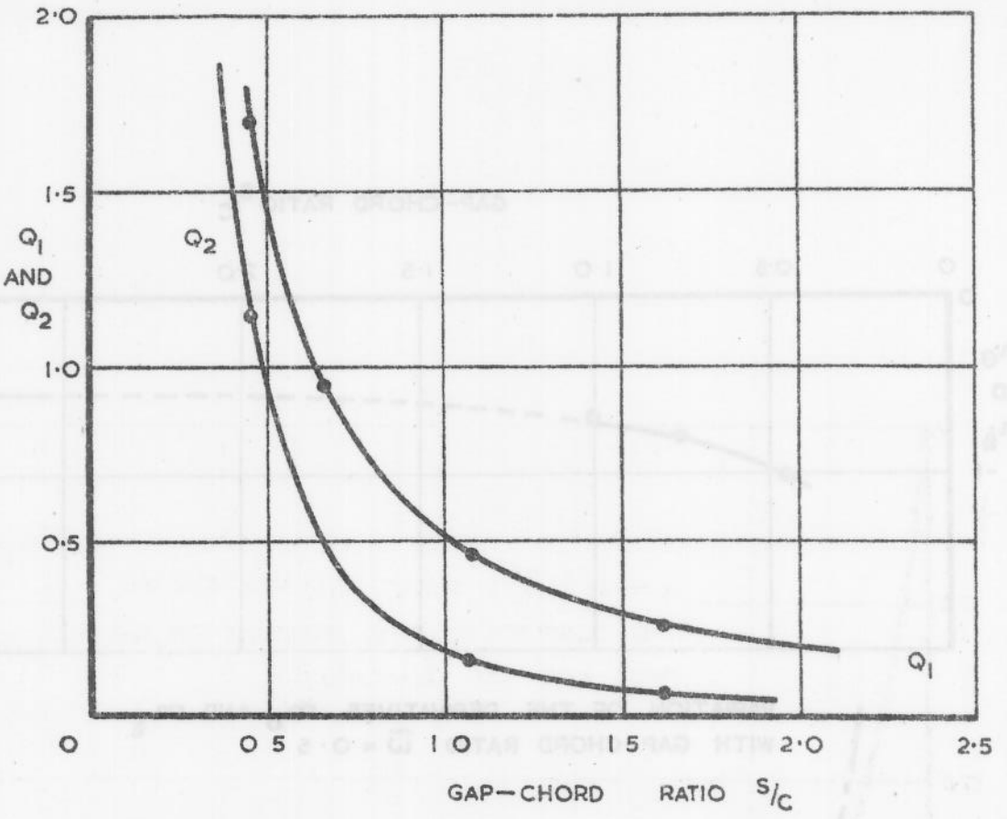

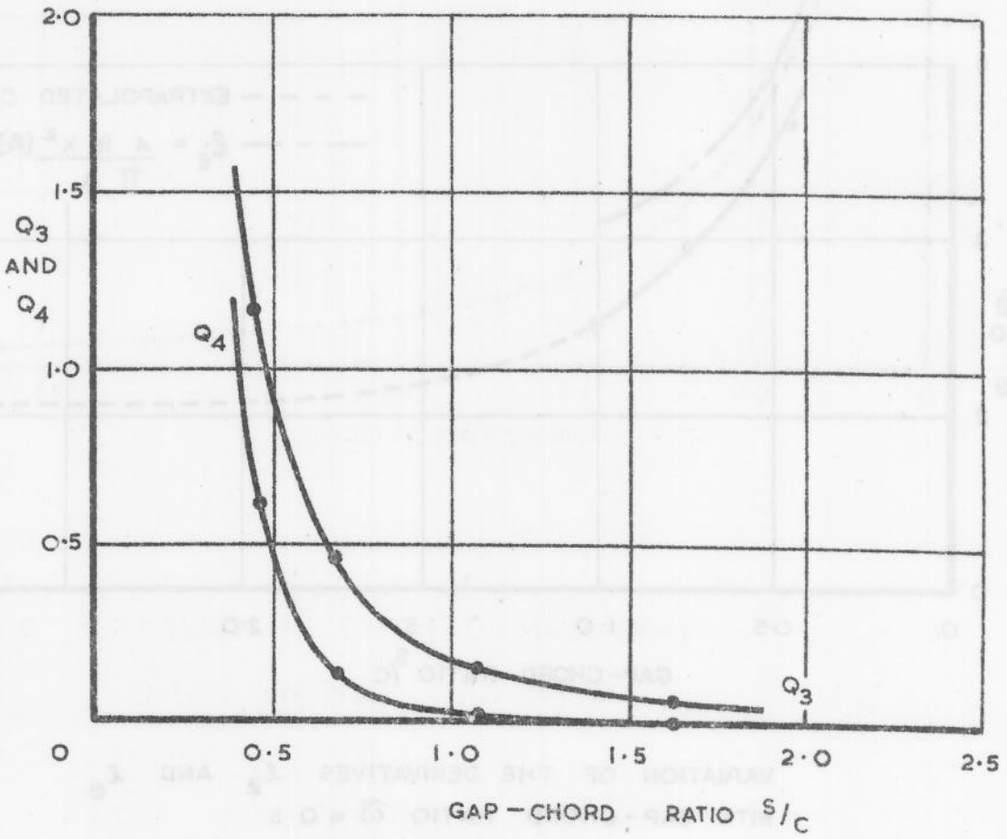

VARIATION OF THE FUNCTIONS Q_1, Q_2, Q_3, Q_4.

FIG. 19.

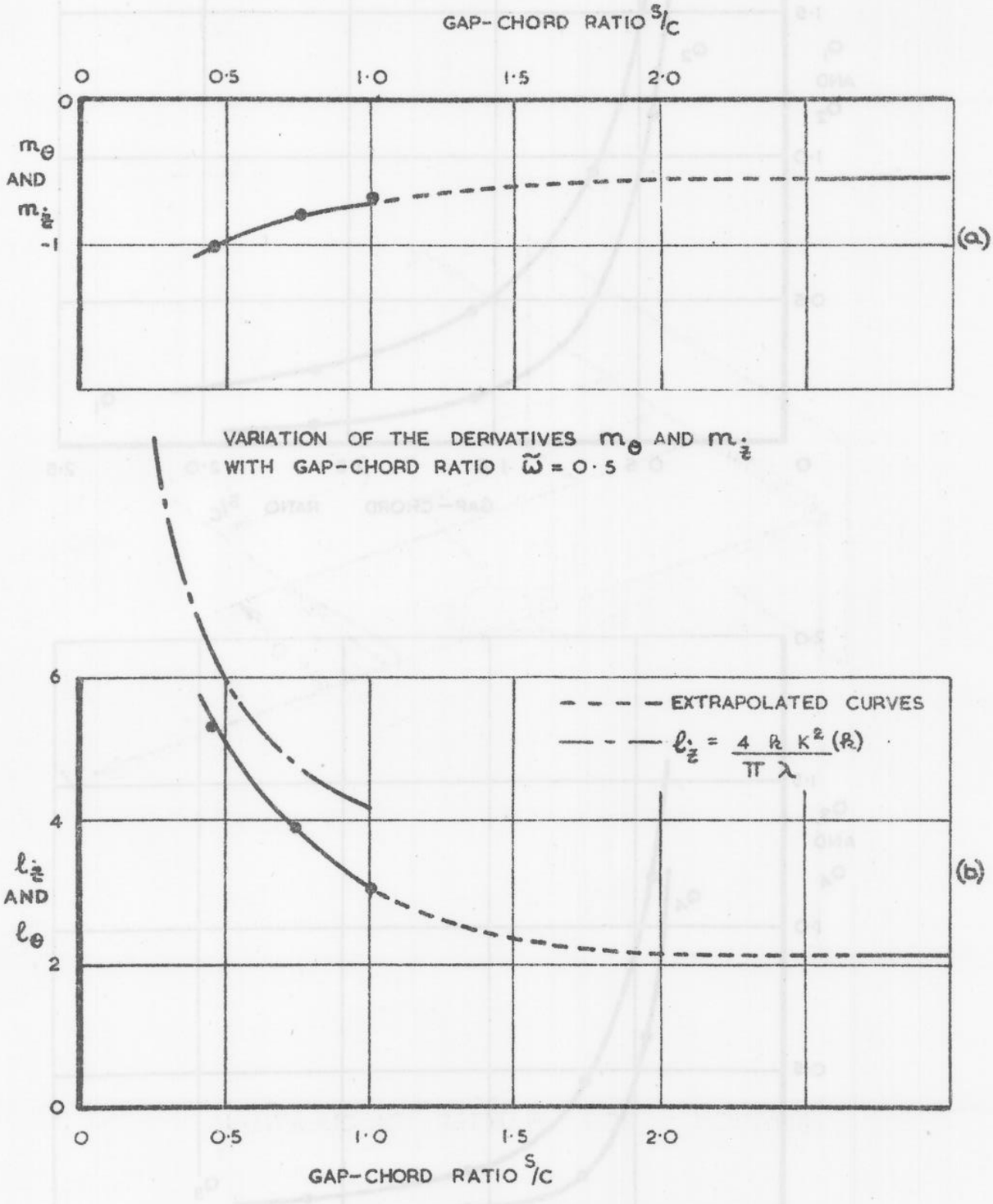

VARIATION OF THE DERIVATIVES m_θ AND $m_{\dot{z}}$
WITH GAP-CHORD RATIO $\tilde{\omega} = 0 \cdot 5$

VARIATION OF THE DERIVATIVES $l_{\dot{z}}$ AND l_θ
WITH GAP-CHORD RATIO $\tilde{\omega} = 0 \cdot 5$

TYPICAL VALUES OF THE CLASSICAL
AERODYNAMIC DERIVATIVES

FIG. 20.

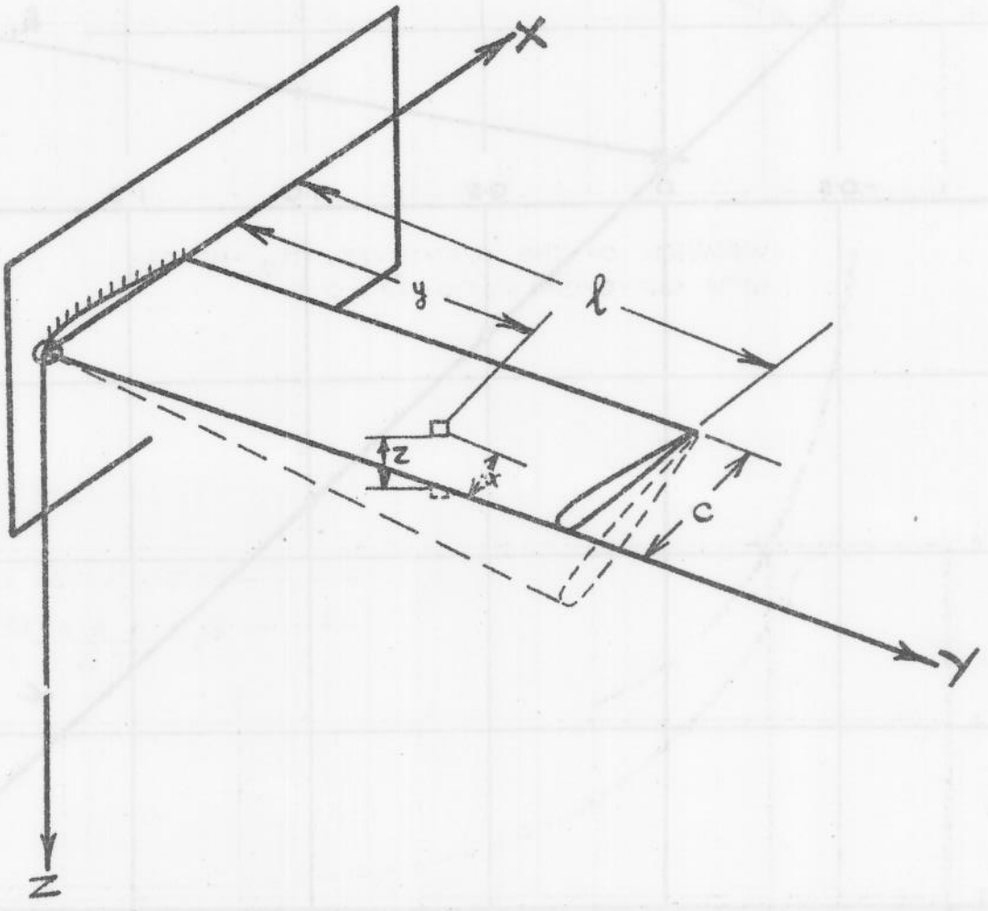

NOTATION FOR FLUTTER CALCULATIONS.

FIG. 21.

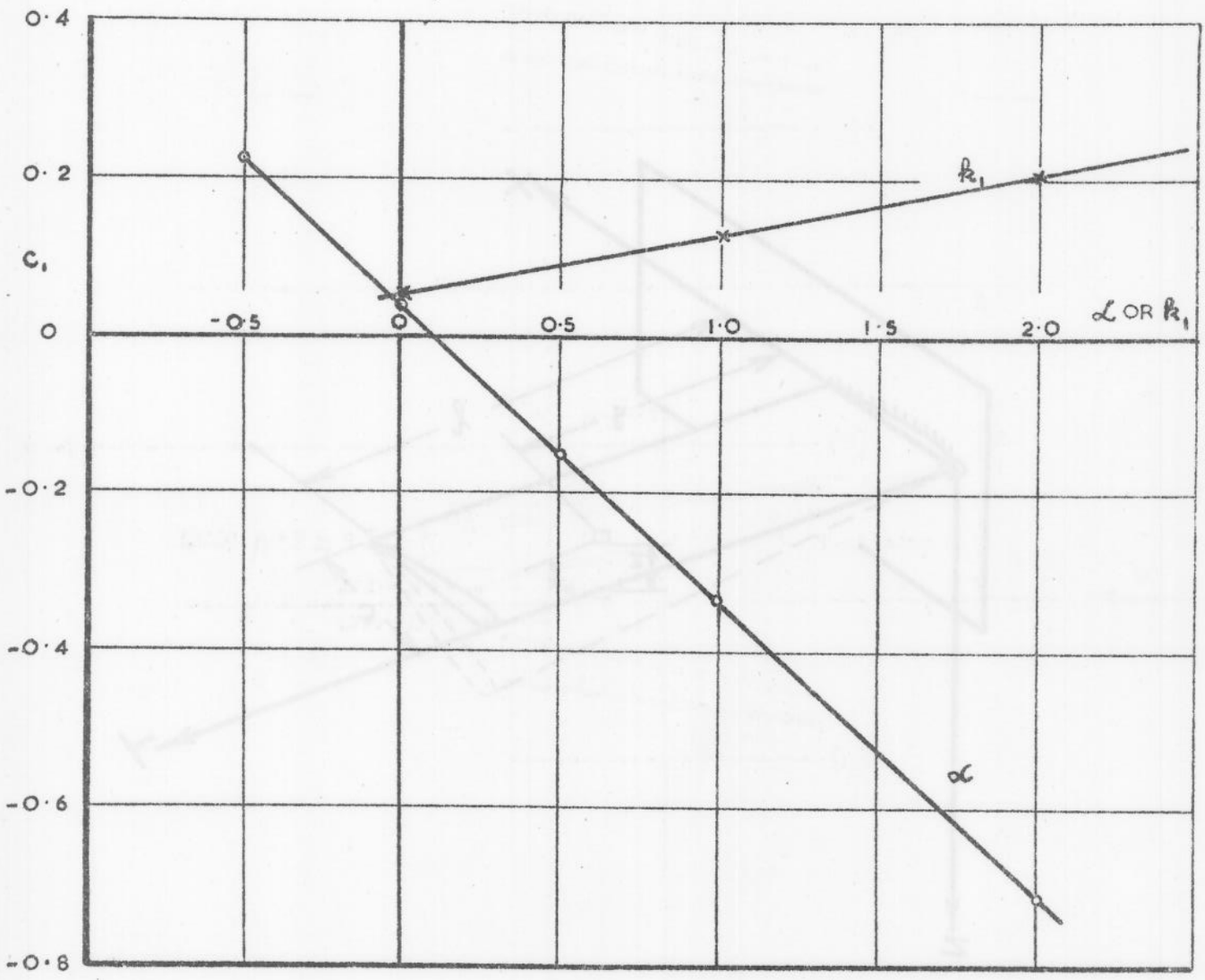

TYPICAL VARIATION OF THE COEFFICIENT

c_1 WITH α AND k_1

FIG. 22.

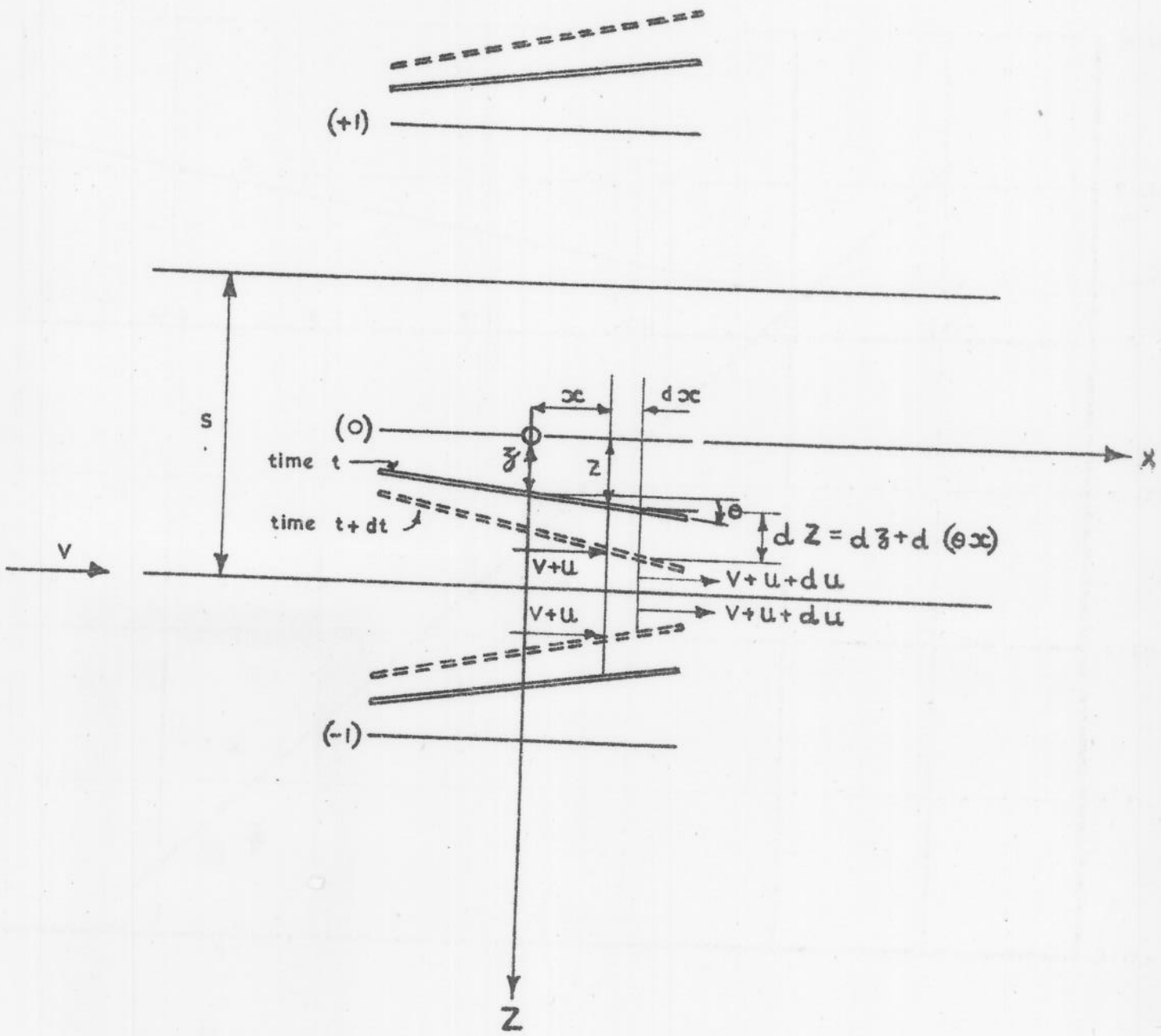

DIAGRAM SHOWING OSCILLATING AEROFOILS IN CASCADE.